UCRL-51872

THE DESIGN OF A REPETITIVELY PULSED MEGAJOULE DENSE-PLASMA FOCUS

O. Zucker
W. Bostick
R. Gullickson
J. Long
J. Luce
H. Sahlin

August 1, 1975

Prepared for U.S. Energy Research & Development Administration under contract No. W-7405-Eng-48

Printed in the United States of America
Available from
National Technical Information Service
U. S. Department of Commerce
5285 Port Royal Road
Springfield, Virginia 22151
Price: Printed Copy $___*; Microfiche $2.25

*Pages	NTIS Selling Price
1-50	$4.00
51-150	$5.45
151-325	$7.60
326-500	$10.60
501-1000	$13.60

Distribution Category
UC-38

LAWRENCE LIVERMORE LABORATORY
University of California/Livermore, California/94550

UCRL-51872

THE DESIGN OF A REPETITIVELY PULSED MEGAJOULE DENSE-PLASMA FOCUS

O. Zucker
W. Bostick
R. Gullickson
J. Long
J. Luce
H. Sahlin

MS. date: August 1, 1975

Contents

THE DESIGN OF A REPETITIVELY PULSED MEGAJOULE DENSE-PLASMA FOCUS

Abstract

This report describes a 1 pulse per second, dense-plasma-focus (DPF) materials-testing device capable of delivering a minimum of 10^{15} neutrons per pulse. Moderate scaling up from existing designs is shown to be sufficient to provide 2 x 10^{13} neutrons/cm^2. s to a suitable target. The average power consumption, which has become a major issue due to the energy crisis, is analyzed with respect to other plasma devices and is shown to be highly favorable. Also discussed is a novel approach to capacitor-bank and switch design with respect to repetitive-pulse operation.

Introduction

GENERAL

To produce a practical design for controlled-thermonuclear or laser-fusion reactors, it is necessary to assume that some structural members will be irradiated by a high flux of 14 MeV neutrons in addition to a "plasma wind" containing gamma-rays, x-rays, ions and electrons. Thus, a necessary preliminary to any final design must be the test and evaluation of the structural materials that will be exposed to this hostile radiation environment. We propose to satisfy the neutron-source requirements for materials testing with a one-megajoule dense-plasma-focus (DPF) system designed to deliver one 10^{15} DT neutron burst per second. (A similar facility sponsored by Euratom for fusion-reactor materials testing is being considered for a joint European plasma-focus effort at Frascati.) The design of the one-megajoule system described in this report offers unique solutions to high-voltage, energy-storage and switching problems for a repetitively pulsed system. It is suggested that the technology described herein can lead to the building of plasma foci in the multi-megajoule range.

The design of the proposed system is based on a one-megajoule nonrepetitive DD plasma-focus device now being constructed in the Physics

Department at Lawrence Livermore laboratory (LLL). This machine, which is jointly funded by ERDA and the Defense Nuclear Agency (DNA), has been given the generic name of Sigma Filippov Geometry (SFG). Because of its efficiency and realistic plasma-wind environment, we suggest that the plasma focus simulator herein proposed can be considered as a device for testing materials to be used in both pulsed laser, DC and quasi DC fusion reactors.

Some salient advantages of the SFG simulator are:

- The plasma focus is at the present time unequaled as a laboratory pulsed-neutron source.
- Because of its approximate E^2 scaling and high-temperature, high-density plasma and point-source characteristics, the SFG simulator should be basically more efficient than other proposed high-energy fusion-reactor simulators. (E is the stored energy of the plasma focus.) This should be an important consideration during the next few years when considering the energy crisis and the power requirements of alternative systems.
- The goals set for the SFG simulator should be attained without any new or fundamental advance in physics. However, considerable development work will be required.
- An R&D program aimed toward fundamental improvements may lead to increased yields in the range of 10^{16} to 10^{17} DT neutrons per pulse.
- In common with other plasma simulators the proposed device provides a realistic environment which includes gamma-rays, x-rays, electrons and ions as well as neutrons. This plasma wind is not provided by present or proposed beam-target systems.
- Because of its large electrode surface area and special geometry, the proposed SFG simulator is easy to cool and provides better radiation areas and easier access than other plasma-focus devices.

The high demonstrated efficiency and small source dimensions of the SFG simulator are major positive considerations. Unless proposed DC and quasi-DC large surface-area sources significantly improve their efficiency (near scientific breakeven),

their power consumption will be in the hundreds or thousands of megawatts in order to achieve the required flux levels. Even if such power demands can be met, (an unlikely possibility considering the energy crisis and the gloomy energy projections for the 1980's) the utility bill for the operation of these devices will be unreasonably high. However, due to the high efficiency and small source size, the neutron flux requirement can be met using the DPF at a small fraction of these costs.

It is assumed that there will be a need for materials testing in the immediate future. This requirement has influenced us to limit our proposal to a simulator design based on the one megajoule nonrepetitive plasma-focus device now under construction in the LLL Physics Department.

DESIGN CONSIDERATIONS

The SFG device currently being constructed at LLL is scheduled to become operational in mid 1975. During the ensuing year it should achieve an operational level of $>10^{13}$ DD neutrons per pulse. This yield is equivalent to a DT yield of $>10^{15}$ neutrons. The pulse width for this high-energy system is expected to be nominally about 100 ns. However, it must be recognized that the high-space-resolution and time-resolution measurements of the Stevens group[1] show that the broader neutron and x-ray pulses (about 100 ns) are really made up of a superposition of a number of short pulses, each of which is about 10 ns long, or less. Thus the actual neutron and x-ray irradiation of a sample which is a few centimeters from the plasma focus is in the form of very short pulses, each one of which is a fairly good simulation of the neutron pulse from a laser fusion device. For testing the effect of 14 MeV neutrons on the bulk of structural materials it is very likely that the accumulated neutron fluence rather than the peak flux is the important factor. Therefore this 1 MJ, 1 pps (pulse per second) plasma focus can also very likely be a suitable simulator for DC and quasi-DC reactors. This plasma focus could also be operated at 60 pps at 150 kJ, if so desired.

The design selected for the nonrepetitive SFG device now under construction eliminates all cables by mounting plasma focus components directly on flat transmission-line plates. This design avoids the damage that occurs when high-voltage transients encounter high impedance at cable connections. A 100 kJ plasma-

focus device which incorporates this feature has been in operation at LLL for 1 1/2 years. It has proved the soundness of the unique cable-less design we plan to use in the SFG fusion-reactor simulator.

It is important to note that the success of this project depends on straightforward technological extrapolation of well-known plasma-focus and electrical engineering parameters. Present plasma-focus devices are designed for intermittent operation which limits them to about 100 shots per day. Thus, a major milestone in building a materials-testing neutron source is the building of a suitable repetitively-pulsed capacitor bank. The development of long-lived electrical components for the repetitive system does require considerable innovative engineering and development work. Items which must be considered include long-lived switches, capacitors and plasma-focus components.

Electrical-Energy Requirements for Neutron-Test Facilities

A major consideration in the evaluation of a fusion simulator is its electrical-power requirements. This section is a review of the energy requirements for plasma driven devices. The efficiency of accelerator beam-target systems are relatively well-known and will not be discussed.

The energy release of 17 MeV due to one DT fusion is 2.8×10^{-12} J. The energy is carried off by these reaction products: a 14 MeV neutron that does not couple to the reacting plasma, and a 3.5 MeV α particle that may be contained in the reacting plasma and thus contributes to plasma heating. The operating power required by a 14 MeV neutron test facility is given by

$$P = \frac{\phi A}{\epsilon} (2.8 \times 10^{-18}) \text{ MW},$$

where

$A = 4\pi R^2 \text{ cm}^2$

R = the test volume radius in cm

ϕ = the 14 MeV neutron flux in neutrons/cm^2.s

ϵ = efficiency defined as the ratio

$$\frac{\text{fusion energy out}}{\text{electrical energy in}}$$

P = electric power in MW required to operate the facility.

If we assume $\phi = 10^{14}$ neutrons/cm^2.s, then

$$P = \frac{A}{\epsilon}(2.8 \times 10^{-4}) \text{ megawatts}$$

The initial estimate of · for D-T for a plasma focus operated at the 1 MJ level is · = 2.8 x 10^{-3}. This estimate is based on experience with the largest DPF operated (at Los Alamos) and the generally accepted yield ratio of 100 for D-T vs D-D. If the radius R of the test volume is taken as 2 cm, then for the proposed pulsed-plasma-focus neutron and radiation facility A = 50 cm^2. It should be noted that small test samples could be placed closer than 1 cm from the plasma-focus neutron source. The power (P) required to operate the plasma focus system with $\phi=10^{14}$ n/cm^2.s, A = 50cm^2, $\varepsilon = 2.8\times10^{-3}$ is 5 MW if no improvements in present system performance are assumed. The research and development program described later in this report may lead to a reduction in P by a factor 2 to 5.

To provide an estimate of operating-power requirements for neutron-test facilities based on various thermonuclear plasma devices we will assume that the condition $n\tau = 10^{12}$ at $T = 8$ kv has been attained. This condition corresponds to a value of · = 0.01 or 1% of Lawson criterion. A value of ε very much smaller than · = 0.01 is probably not feasible because it results in large operating-power requirements. For the conditions $\phi = 10^{14}$ n/cm^2. sec, $\varepsilon = 0.01$, and $n\tau = 10^{12}$ the input power requirement P is given by

$$P = 0.028A \text{ MW}$$

Under these conditions a pulsed plasma-focus test facility with a test volume surface area A = 50 cm^2 would require operating power of 1.4 MW. For comparison, the area of a test facility based on a mirror machine concept has been estimated to be 1.26 x 10^4 cm^2, and thus, for T = 8 kv, $n\tau = 10^{12}$ and $\varepsilon = 0.01$ would require an input operating power of about 350 MW. A neutron-test facility for these same conditions based on a linear theta pinch with A = 1900 cm^2 would require a 53-MW operating-power source. It can be seen that the power requirements for Sherwood-device-based test facilities will be large because these low-density systems necessarily occupy large volumes and thus have considerable surface area. Of course, in principle, the power requirements could be reduced by increasing ε, but to achieve the pulsed-plasma-focus power requirement, a Sherwood-device-based facility would have to approach the break-even condition of $\varepsilon = 1$. If some of the energy could be recovered through direct conversion of high-energy ions and electrons

then these power requirements would be reduced. However, unless near-fusion conditions are achieved, charge exchange between high-energy ions and background gas would reduce the effectiveness of direct conversion.

For completeness, we outline here the determination of ε. The fusion-energy production, E_F, for a 50-50 DT plasma is given by

$$E_F = \frac{N(n\tau)}{4} \langle\sigma v\rangle \ (f\ 2.8 \times 10^{-12})\ \text{J},$$

or

$$E_F = 7 \times 10^{-29}\ fF(T)\ N(n\tau)\ ,$$

where

$10^{-16}F(T) = \langle\sigma v\rangle$ = Maxwell average cross-section

τ = confinement time

n = ion density

V = volume

N = total number = nV

T = temperature (keV).

Also, f is the fraction of the 2.8×10^{-12} J/DT fusion considered available. For example, in arriving at break-even conditions $f = \frac{1}{5}$ because one assumes that only the 3.5-MeV α particle goes into plasma heating, and the 14.1-MeV neutron energy is lost from the system. For present purposes we will assume $f = 1$, i.e. that all of the 17.1 MeV per fusion is the output energy.

The energy required to heat the plasma to T kV, E_H, is given by

$$E_H = \frac{3}{2}\ 2NT(k)\ \text{J} = 4.8 \times 10^{-16} NT\ \text{J},$$

where k = Boltzmann's constant. The energy lost to bremsstrahlung, E_B, is

$$E_B = 5.35 \times 10^{-31}\ Nn\tau T^{\frac{1}{2}}\ \text{J}.$$

We may also write

$$E_B = R(T)\ E_F,$$

or

$$R(T) = \frac{7.64 \times 10^{-3}\ T^{\frac{1}{2}}}{fF(T)}.$$

Now if we require E_F to be some fraction ε of the sum of E_H and E_B, then we obtain

$$\varepsilon E_H = E_F(1-\varepsilon R(T)),$$

or

$$\frac{\varepsilon T \times 10^{13}}{F(T)} = 1.46\ \left(f - \frac{7.64 \times 10^{-3}\ \varepsilon T^{\frac{1}{2}}}{f\ F(T)}\right)\ (n\tau).$$

To obtain the condition for break-even ($\varepsilon = 1$), we assume T = 10 kv and f = 0.2, and F(10) = 1.1, and find $n\tau \approx 3 \times 10^{14}$ which is roughly Lawson's break-even condition ($n\tau = 10^{14}$).

For the present purpose we are interested in $\varepsilon << 1$, f = 1, and 0.1 kv < T < 10 kv. In this range the term $\varepsilon R(T)$ is negligible, and consequently we may write

$$\varepsilon = \frac{1.46 \times 10^{-13}}{T}\ (n\tau)\ F(T).$$

If we let $n\tau = g \times 10^{12}$, then the expression for ε becomes

$$\varepsilon = \frac{0.146 g F(T)}{T}.$$

This is the equation used to determine the ϵ values in Table 1. We can also see how ϵ changes with T for a fixed $n\tau = 10^{12}$, i.e. g = 1. In this case

$$\epsilon = \frac{0.146F(T)}{T}.$$

Values of ϵ from this equation for a range of values of T are given in Table 2.

Table 1. Present experimental parameters

Device	Density n (particles/cm^3)	Confinement Time T (s)	Ion temperature T(kv)	$n\tau$	Calculated values of ϵ
Tokomak (Ref. 2)	1.8×10^{13}	0.01-0.02	0.5	3.6×10^{11}	$\approx 10^{-8}$
Baseball II (Ref. 3)	2.5×10^{9}	0.2-4.0	2	10^{10}	2×10^{-6}
2X (Ref. 2)[d]	5×10^{13}	0.0005	6 to 8	2.5×10^{10}	10^{-4}
θ pinch[b] (SCILAC, Ref. 2)	3×10^{16}	3×10^{-6}	0.3	10^{11}	$\approx 5\times10^{-10}$
Plasma focus[c,e]	5×10^{19}	2×10^{-8}	6 to 8	10^{12}	10^{-2}

[a] An increase in ion temperature by a factor 10 to 5 kv would increase ϵ to 1.4×10^{-3}

[b] An increase in ion temperature by a factor 10 to 3 kv would increase ϵ to $\epsilon = 10^{-4}$.

[c] The actual experimentally determined value is $\epsilon \approx 3 \times 10^{-3}$.

[d] The most recent 2XII results imply an $n\tau$ of $(0.5 \text{ to } 1.0) \times 10^{11}$.

[e] It is still a matter of controversy as to whether or not the neutrons from the high-density mode of the plasma focus are of thermonuclear origin. This debate persists due to a spread that exists in the neutron peak of at most a few hundred kilovolts (the energy peaks at 0° and 90°). From the point of view of materials testing, such deviations from pure thermonuclear behavior are not significant.

Table 2. ε vs T for $n\tau = 10^{12}$

T (kv)	F(T)	ε
10	1.1	1.6×10^{-2}
9	0.8	1.3×10^{-2}
8	0.6	1.1×10^{-2}
7	0.4	8.4×10^{-3}
6	0.25	6.0×10^{-3}
5	0.14	4.1×10^{-3}
4	6.5×10^{-2}	2.4×10^{-3}
3	2×10^{-2}	1.0×10^{-3}
2	3×10^{-3}	2.2×10^{-4}
1	7×10^{-5}	1.0×10^{-5}
0.5	10^{-6}	3.0×10^{-7}
0.3	10^{-8}	5.0×10^{-9}

Design Criteria for the SFG Repetitively Pulsed Material-Testing Device

REQUIRED YIELD FOR RAPID PULSING

The dense-plasma focus produces the largest neutron yield per unit plasma volume of any laboratory device now available. For irradiation of materials, however, it suffers from having a very slow repetition rate. Present day dense-plasma focus devices can be fired only about once every ten minutes. Obviously, for the device to be useful for testing purposes a repetition rate of one or more times a second is needed. To accomplish this goal the dense plasma focus must undergo extensive modifications. For example, the device itself must be cooled as well as the switches and capacitors. The cooling of this device presents stringent engineering problems. However, the designs described in this report appear to provide adequate cooling for the various components.

Present plasma-focus devices have achieved 1.2×10^{12} DD neutrons at 420 kJ stored energy. Figure 1 is an empirical scaling of DD neutron yield N vs stored energy E for most of the plasma-focus machines which

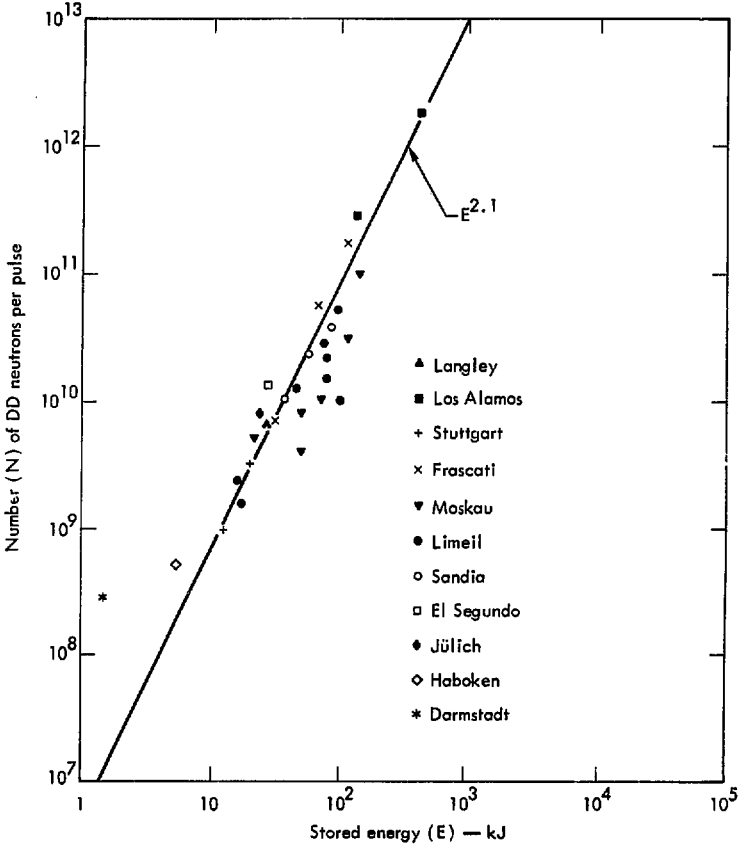

Fig. 1. Neutron yield vs stored energy per pulse for various reactors.

have been operated.[4] These machines span a range in energy (E) of from 1 kJ to 420 kJ and a range in V ($E = \frac{1}{2} CV^2$) of 10 kV < V < 46 kV. The machines with the higher E are designed to have, in general, somewhat larger V, but also larger capacitance (C) and larger total inductance (L). Figure 1 shows an $E^{2.1}$ line drawn through the points. One can see that the scatter of the points about the $E^{2.1}$ line is fairly large, especially for the two machines with the lowest stored energy (E) (Darmstadt and Hoboken). The machines shown in Fig. 1 have been designed according to the experience and taste of eleven different laboratories; no one parameter was kept constant in these various designs. The predicted theoretical scaling according to Filippov and Imshennik[5] when L is increased as C and E are increased is $N \sim E^{1.9}$. This predicted law agrees reasonably well with the $E^{2.1}$ line which has been drawn on Fig. 1 when one considers that the data of Fig. 1 came from eleven laboratories where the values of C and V were chosen at will.

However, the Bennett pinch relationship that $I^2 \propto NkT$ and the fact that the magnetic energy available is directly proportional to I^2 suggests that the most important factor in directly determining N is I, not V or E, and therefore the scaling of N vs I should be the most meaningful of all scaling relationships. Figure 2 shows N vs I for each of the machines for which we could obtain the appropriate value of peak current. It can be seen that the points lie fairly well on a $N \propto I^5$ line. The theoretical arguments of Filippov and Imshennik[5] state that when a plasma-focus system remains optimized and L and C remain constant, one should expect $N \propto E^{2.43}$ or $N \propto I^{4.9} \propto V^{4.9}$. The agreement between the empirical and theoretical values of the exponent here is fairly good. The two very small Darmstadt and Hoboken plasma-focus devices, however, lie considerably above the I^5 line as shown in the N vs E and N vs V plots by the Darmstadt group[6] (Fig. 3). The line drawn through the data for this small machine indicates $N \propto V^8$, which implies $N \propto I^8$. Also note how both the Darmstadt machine and the small Hoboken machine (which are very similar; the Darmstadt machine uses an electrode structure identical to that of the Hoboken machine) lie considerably above the I^5 line in Fig. 2. The implication of these data is that small machines with their more concentrated magnetic fields are basically superior to the

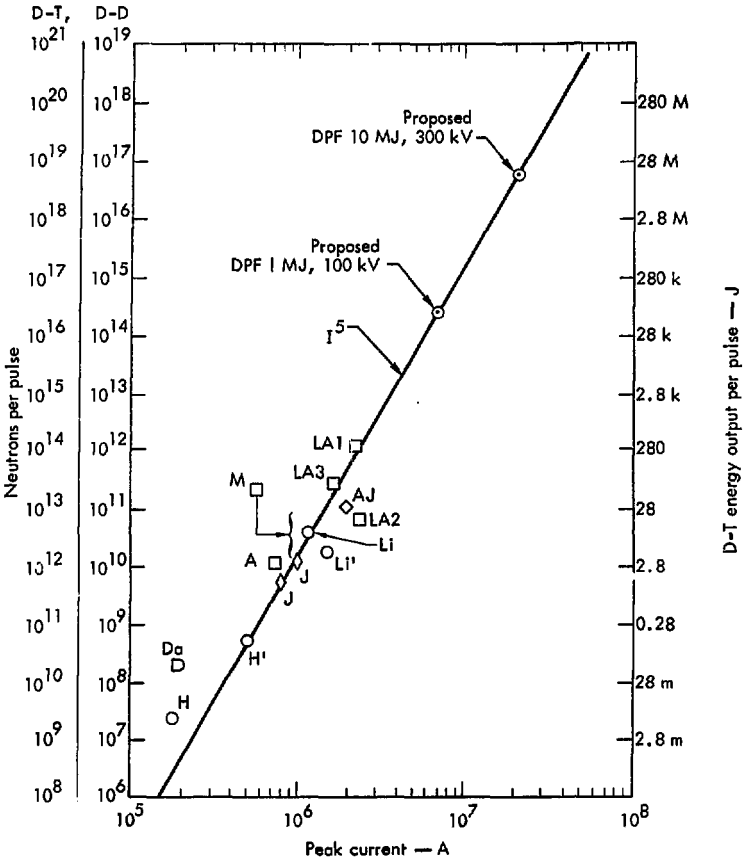

Fig. 2. Neutron yield vs peak current per pulse, and corresponding energy output.

Legend for Figure 2

AJ Aerojet Nucleonics. 250 kJ, 20 kV, 320 μF.

Da Darmstadt. 0.34 - 1.35 kJ; 10 - 20 kV; C = 6.7 μF; inductance = 24 nH; circuit frequency = 400 kHz; Mather type gun length = 10 cm, diam = 5 and 1.6 cm.; hollow center electrode. See Ref. 6.

H Hoboken. Electrode structure is identical to that of Darmstadt group. 14 - 18 kV; C = 6 μF; hollow center electrode. Now in operation at University of Buenos Aires. See Ref. 1.

H' Hoboken. About 5 kJ; 45 μF; 14 kV; time to current peak 1.8 μsec; Mather type gun; length = 14 cm, diam = 10 cm and 3.4 cm. Hollow center electrode.

A^E Aerospace Corporation.

J Julich. 25 kJ; 40 kV; C = 22.4 μF; center electrode 3 cm long; 6 cm diam; outer electrode = 11 cm diam.

Li Limeil. 96 kJ, 40 kV, inductance = 27 nH; 1/4 cycle time = 2.5 μs.

Li' Limeil. Plasma focus driven by explosive generator.

LA^1 Los Alamos. DPF-6; 420 kJ.

LA^2 Los Alamos. DPF-5; 120 kJ.

LA^3 Los Alamos. DPF-6; 210 kJ.

M Moscow. $Y \rightarrow 10^{10}$ to 10^{11} DD neutrons; I = 1 MA.

larger machines. Although the data are still scanty, the message seems to be that the best design procedure is to use very high V (several 100 kv), low L (and $\dot{L}$), and relatively small C to obtain high current. In doing so the designer can perhaps enjoy a scaling law even better than $N \propto I^5$. Figures 4 and 5 show Los Alamos N vs V data for a 212 kJ machine, which shows a $N \propto V^5$ ($\propto I^5$) when the pressure was kept constant and $N \propto E^2$ ($\propto V^4$) for DPF-5 and DPF-6 (Ref. 7) when the neutron yield is optimized by changing the pressure.

The SFG plasma focus proposed here is calculated to have a peak current of 7 MA at V = 100 kv and E = 1 MJ. This machine will produce, according to the I^5 scaling, 3×10^{16} DT neutrons per pulse and about 85 kJ in nuclear energy per pulse (17 MeV = 2.8×10^{-12} J per DT reaction). If the voltage V (and I) are raised by

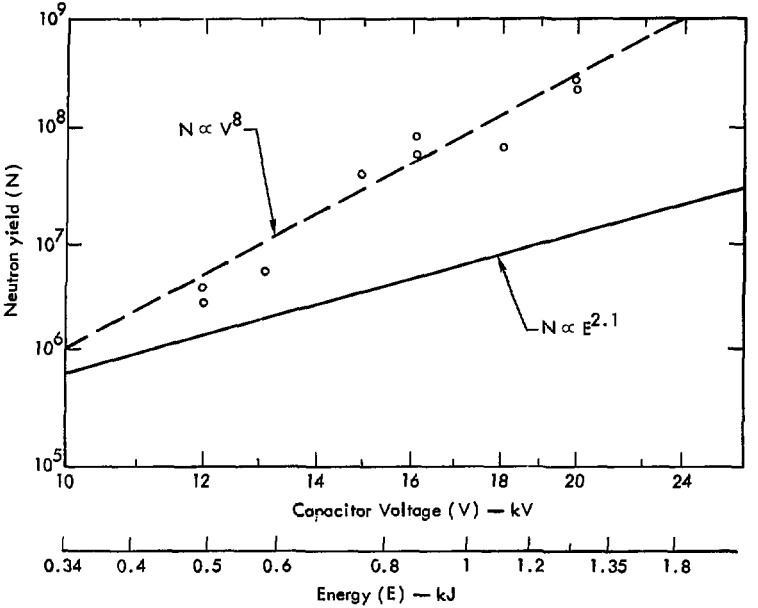

Fig. 3. Neutron yields in relation to capacitor energy (E) and voltage (V) in Darmstadt machine.

a factor of 3 to V = 300 kV (I = 21 MA), the output is 6.5×10^{16} DD neutrons per pulse = 6.5×10^{18} DT neutrons per pulse = 18 MJ per pulse. The nuclear energy released per pulse will thus exceed E (input energy) by a factor of 2.

With the recycling of about 50% of the energy (about $\frac{E}{2}$ left in the storage capacitance after each cycle) at 1 pps the average power consumed for the 100 kV, 1 MJ operational level will be 0.5 MW. The average neutron production will be 3×10^{16} neutrons/s, which is an average output power of 85 kW. Thus, on the average it operates at 17% of break-even. The capacitors and switches of the proposed bank must be designed conservatively enough to stand a repetition frequency of more than 1 pps. Therefore, if the user so desires, an

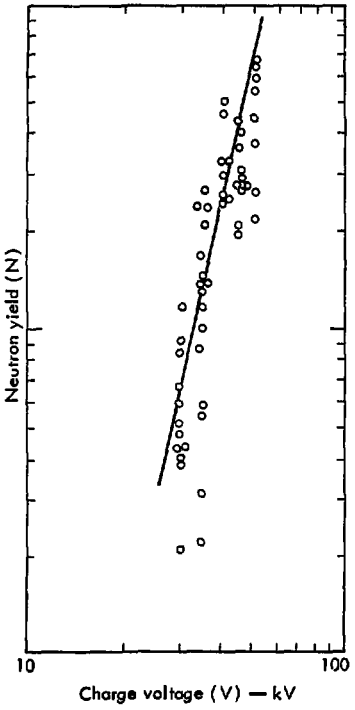

Fig. 4. Neutron yield vs charge voltage (Los Alamos DPF-6) (Ref. 7).

average yield of 3×10^{16} DT neutrons/s can be attained. The capacitor is also designed to operate at V = 300 kV at reduced repetition frequency. The user could then expect about 7×10^{18} neutrons per pulse.

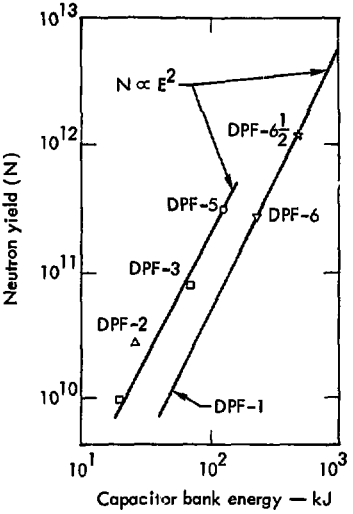

Fig. 5. Neutron yield vs capacitor bank energy (Los Alamos reactors).

The plasma focus will remain a point source. However, the Sigma Filippov (SFG) device proposed by LLL circumvents the well-known window and access problems which have seriously curtailed the usefulness of the coaxial DPF as a testing device. The decision of the Euratom fusion group to use a Filippov-type, repetitively-pulsed plasma focus for material testing was very probably founded on similar considerations.

The LLL SFG now being designed will be used for exploratory research work and component testing for the proposed rapid-pulse system. However, when such a testing device is built it must have well-cooled electrical components, remote handling, control systems, a high-capacity power supply, a tritium handling facility and about six feet of radiation shielding.

ENERGY COUPLING TO PINCH

As stated earlier, we would like to maximize the current in the machine. Before we solve the circuit equations in detail we can make some general observations.

Let us assume that the plasma sheet runs down with a constant velocity and that the gun's inductance L_g varies linearly with distance and thus with time. If a constant voltage source V is applied across such a linearly changing inductance, we will obtain a constant current $I = V/\dot{L}$ where $\dot{L} = dL_g/dt$. Thus maximizing V and minimizing $\dot{L}$ will maximize the current. $\dot{L}$ can be minimized by reducing the gun's inductance and increasing the rundown time. The rundown time can be increased by increasing the gas pressure. However, it has been shown experimentally that rundown time should be less than 3 μs.

If the residual inductance L_B is not zero as assumed earlier, then it will limit the current, since in a purely inductive circuit we have $V\tau = L_B I$. Thus, reducing L_B and increasing V and τ will increase the current. With these considerations in mind, we designed a high V, low L_B, low $\dot{L}$ system which will maximize the current while keeping the energy reasonably low. The following is a more detailed analysis of the circuit utilizing a constant $\dot{L}$ for the machine and showing computer plots of the results of more sophisticated geometries.

In the solution of the circuit in Fig. 6 the peak current I_m for the plasma focus is not simply related to V_o, C_B or L_B, where the subscript B refers to the bank. One must recognize that as the current sheath moves, there is an $\dot{L}$ term and thus the

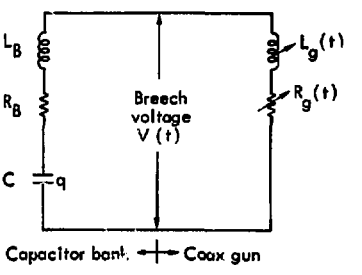

Fig. 6. Equivalent circuit of coaxial plasma gun.

circuit of Fig. 6 is an attempt to take this fact into account. L_g and R_g refer to the inductance and resistance of the focus electrodes and plasma as seen from the breech, and V(t) is the breech voltage. The appropriate differential equation is

$$\frac{d^2Q}{dt^2} + \frac{(R + \dot{L})}{L}\frac{dQ}{dt} - Q/_{LC} = 0$$

where $R = R_B$ and R_g and $L = L_B + L_g$. Note that the $\dot{L}$ term acts like a resistance as far as its effect on the circuit current is concerned. Where L does not change, the solution is oscillating (the underdamped case) for $R < 2(L/C)^{1/2}$ and decays exponentially for $R > 2\ (L/_C)^{1/2}$ (the overdamped case). The breech voltage V(t) is given by

$$V(t) = R_gI + \frac{d}{dt}L_gI = (R_g + \dot{L})\ I + L_g\dot{I}$$

and the power delivered at the input of plasma focus electrodes is

$$W(t) = IV(t) = R_gI^2 + \dot{L}_gI^2 + L_gI\dot{I} = \underbrace{R_gI^2}_{1} + \underbrace{1/2\ \dot{L}_gI^2}_{2} + \underbrace{\frac{d}{dt}\ (1/2\ L_gI^2)}_{3},$$

Term 1 (above) is the rate of ohmic heating in the electrodes and the nonmoving plasma; term 2 is the rate of doing mechanical work on the plasma; term 3 is the rate of increase of magnetic field energy inside the region between the two electrodes. Thus, $1/2\ \dot{L}_g$ represents the equivalent resistance of the current sheet by virtue of its motion.

It can be shown that of the power delivered at the breech, at most one half (i.e., $1/2LI^2$) can be delivered to the plasma, and of that a half will be directed kinetic energy, the remaining being heat if the "snow plow" velocity is constant in a coaxial gun. With the assumption that the total resistance $(R_B + R_g)$ is constant and $\dot{L} \neq 0$ but $\ddot{L} = 0$, a solution can be obtained. This solution is applicable to the rundown phase of the operation of a coaxial plasma focus.

Shown in Fig. 7 are plots of current vs time (t/t_B) in terms of $I/_{I_B}$ for several values of u_o. The following definitions apply:

$$u_o = \frac{2(L_B/C)^{1/2}}{\dot{L}}$$

$$t_b = \frac{\pi}{2(LC)^{1/2}}$$

(time for the shorted-breech current to reach a maximum)

$$I_b = V_o(C/_{L_B})^{1/2}$$

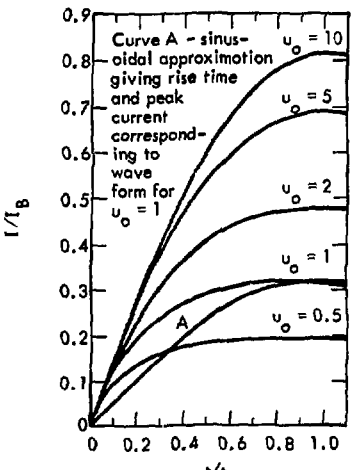

Fig. 7. Normalized current I/I_b vs normalized time t/t_b for various values of $u_0 = 2(L_b/C)^{1/2}/L^*$ for the case $R_t = 0$.

(maximum current when breech is shorted and $R_B + R_g = 0$)

V_o = Capacitor voltage at $t = 0$

If we define I_m as the value of I at its maximum, it can be seen that for large values of u_o, $I_m \to I_B$ and the time of $I = I_m$ approaches t_B. Since u_o is the ratio of the characteristic bank impedance, $(L_B/C)^{1/2}$, to the effective resistance 1/2 L^* produced by the velocity of the plasma sheet, strong damping effects are expected for $u_o < 1$.

Curve A in Fig. 7 shows the sinusoidal current waveform which gives the same peak current and rise time as the more exact expression (for the case $u_o = 1$). The curve illustrates that for values of u_o near to and less than 1 the current, and the rate of work on the plasma, can be considerably greater than that estimated on the basis of a sinusoidal approximation.

Solution of the circuit equation of the combined bank-gun system shows that the attainable peak current I_m is strongly affected by the relative impedance of the bank and gun. To a reasonable approximation,

$$I_m = I_B F(u_o)$$

where $F(u_o)$ is a function which increases monotonically to 1.0 as u_o increases to values much above 1. $F(u_o)$ is shown in Fig. 8. The condition $u_o = 1$ is analogous to the condition for critical damping in an ordinary L-R-C circuit.

Although I_m/I_B decreases with u_o, I_m is actually increasing. This is seen by noting that $u_o \propto L_B^{1/2}$ and $I_B \propto 1/L_B^{1/2}$, so that

$$I_m = I_B F(u_o) \propto F(L_B^{1/2})/L_B^{1/2}.$$

Since the numerator varies more slowly than the denominator, I_m is larger

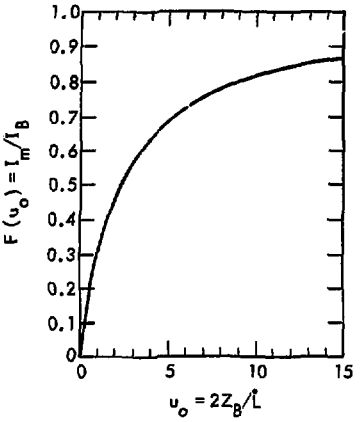

Fig. 8. Maximum gun current divided by maximum bank current vs bank impedance divided by gun impedance for a coaxial plasma gun.

when $L_B^{1/2}$, and thus u_o, is smallest. A rough estimate (good to about ± 25%) gives

$$F(u_o < 1) \approx 0.4\ u_o.$$

Thus, in this range, maximum current is

$$I_m(u_o < 1) \approx 0.8\ V_o/\dot{L}.$$

This result agrees in general with the result for the constant-voltage case. The foregoing discussion assumed a constant velocity rundown in a coaxial geometry. Making the same constant-velocity assumption in the SFG yields $\dot{L} \propto \frac{v}{r}$ where v is the sheath velocity and r is the instantaneous radius of the sheath. A possible further modification is to monotonically decrease the electrode spacing in the SFG thus obtaining an even smaller $\dot{L}$. Figure 9 shows these three basic geometries and their inductance-vs-time curves.

Figure 10 shows the results of a computer calculation of the proposed capacitor-bank source for various inductance vs time curves of the load. It is important to realize that the final collapse in the coaxial system really corresponds to the later stage of the Filippov pinch. Thus, the proper comparison of current should be where the SFG radius equals the inside coaxial-gun radius. The corresponding values (I_m) are 6 MA for the coaxial gun and 7.8 MA for the Filippov geometry. The continued current decrease beyond this point does not represent a decrease in stored magnetic energy until point "B" in Fig. 10. After point "B" in time, a radial collapse of the current sheath occurs causing a great increase in energy density. However, the rate of work done on the plasma exceeds the rate of energy input from the bank, and the total energy in the gun decreases. During the rundown and the early part of the pinch, flux is conserved. Anomalous resistance

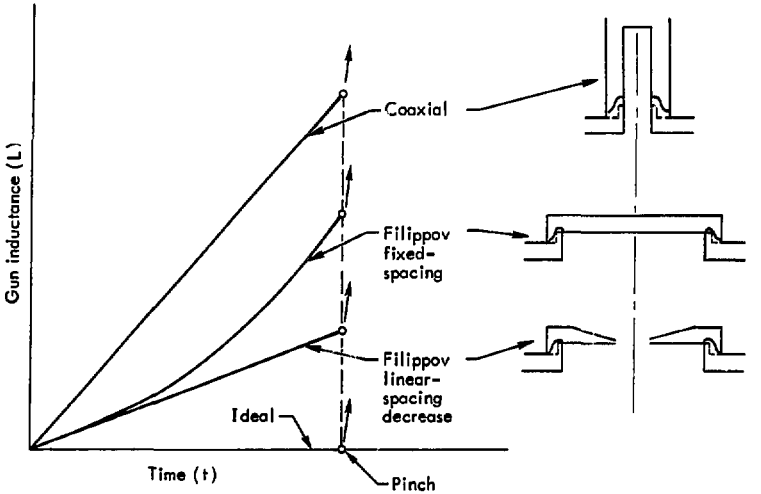

Fig. 9. Inductance vs time for various geometries.

(flux destruction) occurs later in the pinch.

SIGMA FILIPPOV GEOMETRY

The foregoing discussion illustrates some basic characteristics of the DPF which can be exploited in the SFG we are proposing for use in material and component testing. The proposed SFG electrode structure is shown in Fig. 11 and is discussed in detail in the paragraphs that follow.

Inductance Time-Dependency

In a coaxial gun the increase in inductance in the rundown phase is linear with distance. Therefore, if the plasma sheet progresses at constant speed there is a constant rate of inductance increase with time. In the Filippov there is a radial rundown. Since the inductance varies with the log of the radius, $\dot{L}$ will vary with r^{-1}. For a constant-velocity rundown, this behavior is shown in Fig. 9. Initially, the SFG inductance varies slowly, and thus $\dot{L}$ is small at the time the voltage on the capacitor is largest, thus allowing for a rapid buildup of current. *Eventually, close to* pinching, $\dot{L}$ becomes very large but

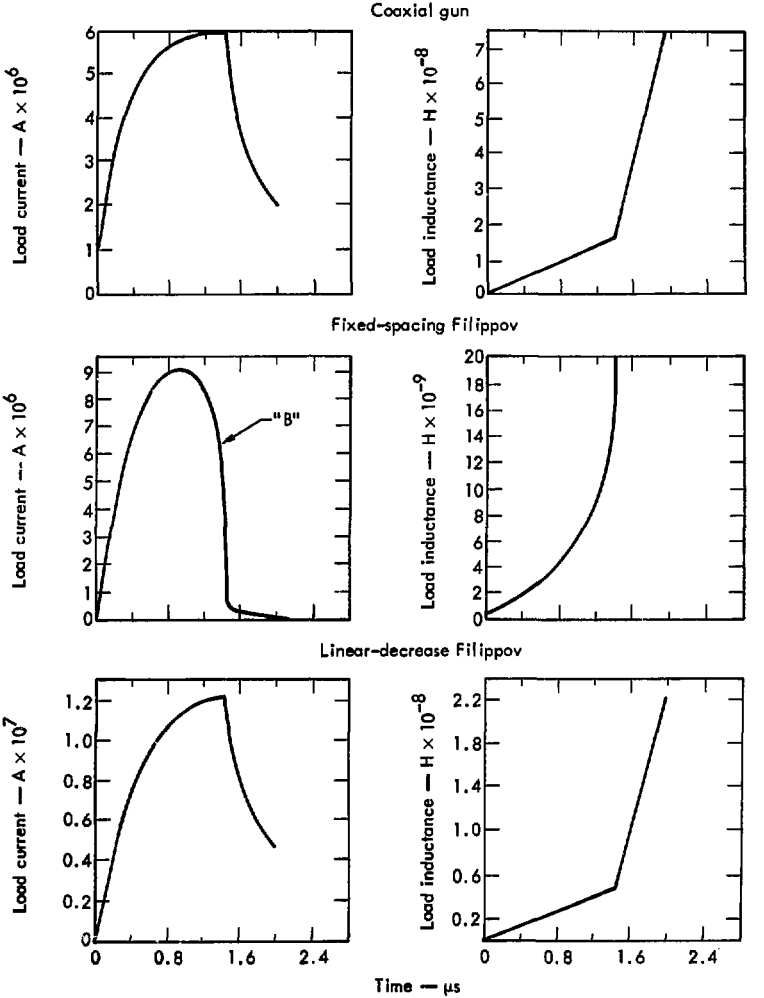

Fig. 10. Calculated load current for various inductance vs time curves of the load.

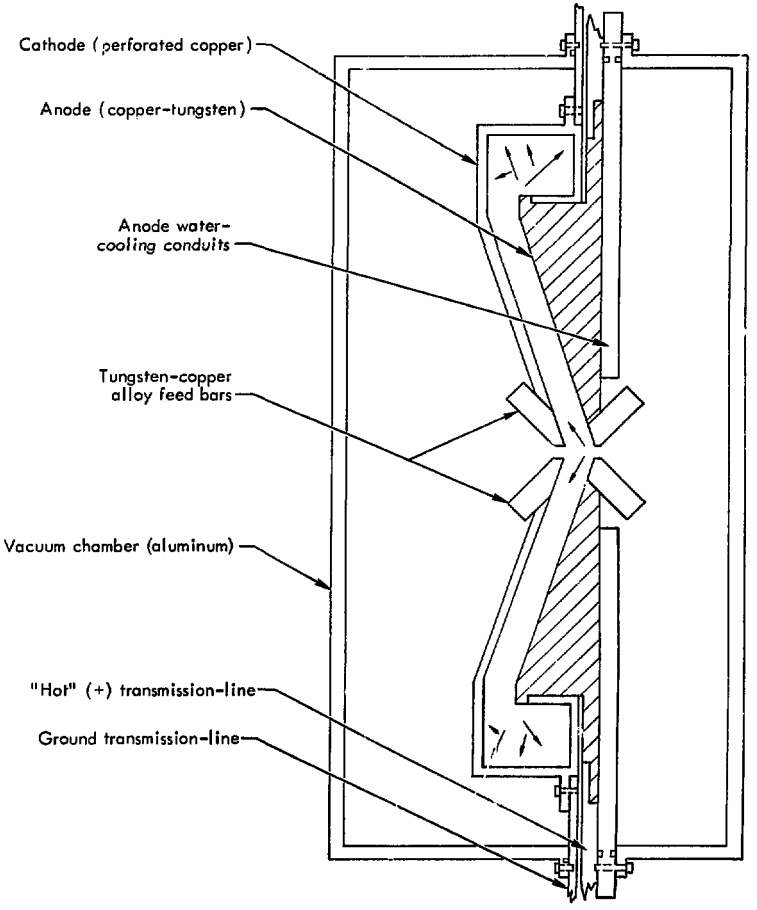

Fig. 11. Sigma-Filippov-geometry (SFG) electrode structure showing tungsten-copper alloy feed bars at locations of high current density.

this happens after the gun has received most of its energy from the capacitor and therefore doesn't affect the energy transport to the gun. A Filippov geometry with monotonically decreasing spacing is also shown in Fig. 9. This geometry affords the highest current buildup.

Low Initial Current Density

A 1 MJ coaxial gun would have a center (anode) electrode about 9 to 10 inches in diameter, whereas a Filippov device of the same energy would be more than three times as large. Thus, the breech-current density of the Filippov gun would be about 30 percent of the coaxial gun for the same energy. This reduced current density will decrease problems of insulator erosion and restrike.

Large Target Area and Plasma-Focus Accessibility

One of the major limitations in utilizing the plasma focus as either a neutron or x-ray testing device is the destructive character of the effluent from the focus and the difficulty of placing samples near the focus. This has become known as the "window" problem. The SFG has greatly reduced these limitations. Reference to Fig. 11 shows how samples can be placed on either side of the focus in the SFG. To avoid effluent damage, metal foils could be transported across the electrode aperture to isolate the samples from unwanted radiation. We have conducted experiments with rolls of deuterated polyethylene (CD_2) foil where a new surface is exposed on each shot. There are no basic technological problems in producing foils with equal mixtures of CD_2 ard CT_2. Heavy metal foils would be useful in those cases where enhanced x-rays are desired.

With a one-meter-diameter center electrode, samples of various sizes can easily be positioned to within a few centimeters of the focus in a region outside of the discharge chamber and, therefore, uncontaminated by tritium. Or, for large-area irradiations of test reactor wall materials in a realistic plasma environment, the center electrode can be made of the test material and receive the full plasma and x-ray bombardment in addition to the neutron irradiation. At a neutron yield of 3×10^{16} per shot, areas of a few square centimeters can be irradiated to 6×10^{14} neutrons/cm^2 per shot. This presupposes a distance of 2 cm from a point neutron source. At 1 pps, the sverage neutron flux would then be 6×10^{14} neutrons/cm^2.s. If the

tests require 10^{14} neutrons/cm^2.s, the test sample can be placed 5 cm from the source.

Cooling

In a rapidly pulsed plasma-focus device, essentially one-half of the megajoule of stored energy released once per second ends up as heat somewhere in the system. The greatest fraction of this heat is deposited in the electrodes and the walls, and must be dissipated to keep system temperatures within allowable limits. For a one-meter diameter conventional Filippov geometry, as the current sheath collapses during the bank quarter-cycle-time of approximately 3 μs, the energy is distributed in a fairly uniform fashion over the surface of the plates forming the electrodes. An exception to this is in the region about 5 cm in radius at the center where the current density becomes very high. If the entire megajoule were deposited in one copper disc a meter in diameter and 1 cm thick, the temperature would rise about 1 degree C. Thus, for continuous operation, coolant flow is necessary.

With water as the coolant and allowing a 10^{o} C temperature rise, the required flow rate is about 400 gallons per minute. This could be accomplished by having cooling water flow inside the anode and cathode electrodes (Fig. 12). The heated water would then be cooled in a heat exchanger and recirculated. The thickness of the cooling water layer would not be sufficient to appreciably alter the neutron spectrum through thermalization. Furthermore, small test samples can be placed very near the plasma focus without any water intervening between the sample and the neutron source.

The center regions of the electrodes, where the radius is less than about 5 cm, are made up of radial tungsten bars to reduce erosion. These bars (see Figs. 11 and 12) can be repositioned as they erode. The tungsten bars which form a portion of the electrodes are designed to have a 3-cm-radius hole in each electrode, reducing the current densities at the electrode surface at the time of maximum pinching. Indeed, for center electrodes without holes, in the Mather coaxial geometry, the "pinch" is observed to dig a hole in the end of the center electrode in only a few shots. At high current levels the rims of the holes will be subject to erosion and with repetitive pulsing the energy dissipated per cm^2 in this region will be high (about 1 kW/cm^2).

The electrode structures should be constructed in a manner which will permit the bu[illegible]f the "snowplowed" plasma, during the rundown, to leak

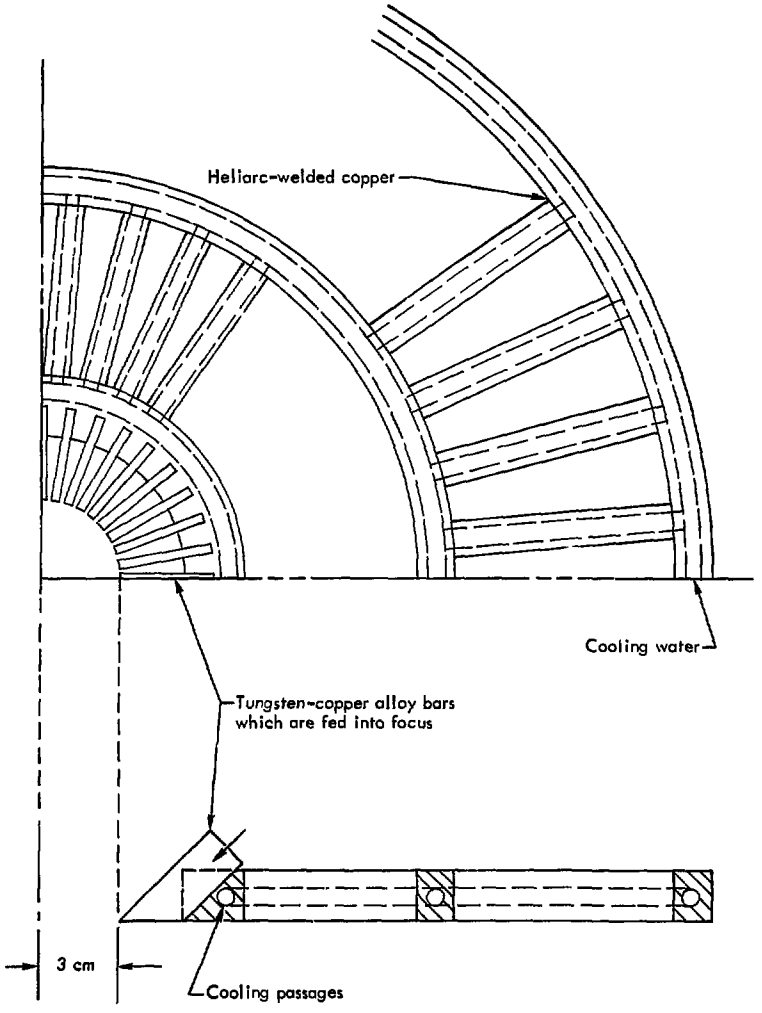

Fig. 12. Construction of outer electrode with slots to permit escape of driven plasma during rundown. Construction shows water cooling labyrinths.

out through perforations or slots in the cathode electrode (see Fig. 12).

Shielding

The electrodes in a dense-plasma focus are highly immune to neutron radiation since they are made from the best materials available, such as tungsten and tungsten alloy. The insulator at the breech however will suffer from radiation damage if not properly shielded. The Σ shape of the electrode was designed to allow tucking the insulator behind massive shielding, thus protecting it from radiation damage, as shown in Fig. 11.

It thus appears reasonable that a plasma-focus testing system based on the SFG concept could be developed to produce > 10^{16} neutrons per second over long periods of time. A factor of major importance is that no highly uncertain extrapolation of yields or basic physics is required to reach the goals indicated. The problems, while very tough, are primarily technological in nature. It is obvious, however, that a vigorous research program on our present SFG device could well lead to significant improvement in the performance of an actual testing device.

STEPPED INDUCTOR

In a high-voltage DPF, voltage-pulse shaping will probably be necessary. Pulse shaping will permit application of bank voltage to the load in a gradual manner. The formation of the current sheath then takes place under low-voltage stress conditions. Only after the current sheath lift-off has occurred is the full voltage applied to the load.

To provide pulse shaping, a non-linear impedance is put in series with the load. The impedance is initially high relative to the load and gradually decreases (in approx. 0.2 μs) to a small value relative to the load. A saturable ferromagnetic material is ideally suited to this requirement. A core made of 1-mil thick 50-50 nickel-iron tape (or Hypersil), 2 cm high, with an inner radius of 1m and outer radius of 1.67 m (properly sectioned and gapped) will adequately satisfy this requirement.

Energy Supply and Capacitor Bank

INTRODUCTION

There are several special requirements that must be met by a capacitor-bank used in a pulsed system. The bank must deliver in a few microseconds at least 1 MJ of energy at 100 kV once per second for upwards of 10^7 shots. A continuously operated 1 MJ, 100 kV, 200 uf, low-inductance (about 5 nh) capacitor bank introduces considerations that are usually neglected in the design of a single-shot capacitor bank such as is used in all of the currently operated plasma-focus machines. Continuous operation at 1 pps requires that component lifetimes be increased by several orders of magnitude. The problem of heat dissipation by the components becomes of great importance and must be an integral part of the design. The low inductance requirement of the design will be difficult to achieve with current techniques, as the volume of the bank will be greater.

In order to see how all of these considerations are interrelated let us consider first the high voltage requirement. The maximum permitted electric field between the foils of a capacitor is approximately 160 MV/m (=4kV/mil). In the staggered foil construction normally used, at this electrical stress corona from the sharp edges of the coil carbonizes a path between the foil edges. See Fig. 13. This corona limits the lifetime of the capacitor to about 1000 shots.

With continuous operation at 1 pps, millions of shots will be required. Hence, the capacitor design must use an electric field low enough to eliminate the corona, namely 40 MV/m (=1kV/mil).

Since the electrostatic energy density is proportional to the square of the electric field, the reduction of the electric-field stress in the dielectric from 4kV/mil to 1kV/mil will require a 16-fold increase of the volume of the capacitor dielectric in order to store the same amount of energy.

A small fraction of the energy stored in a capacitor is dissipated as heat in the conducting foils because of the high currents which flow when the capacitor is discharged. With continuous operation at 1 pps, conventional capacitors would soon succumb to thermal runaway and be destroyed. Obviously the surface-to-volume ratio of the capacitor units must be greatly increased. The question now confronts the designer: Can such a large high-

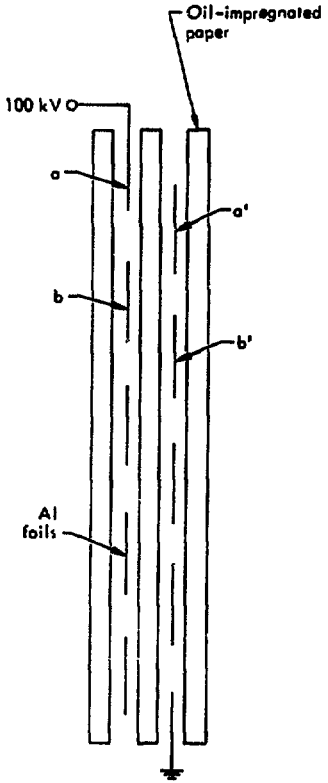

Fig. 13. Staggered-foil-construction capacitor.

voltage capacitor with large surface-to-volume ratio be built and still satisfy the low inductance requirements? The answer is yes. But in order to achieve this goal the design must utilize new and improved techniques which are not customarily available in conventional capacitor design.

THE CAPACITOR BANK

Foil Geometry and Corona Reduction

The pertinent capacitor bank design parameter goals are E = 1 MJ, V = 100 kV, average power = 1 MW at 1 pps, capacitance = 200 μf with a series inductance of less than 5 nH.

The staggered-foil construction of a conventional, high-energy, high-voltage capacitor is shown in Fig. 13. In this figure, oil-impregnated paper separates two sets of foils mounted in a staggered fashion. Effectively, the foils represent a group of capacitors connected in series. In Figure 13, if the voltage between foils a and a' is V, then the voltage between a and b is 2 V. Furthermore, the voltage between a and b is not through the oil-impregnated paper but is along the surface of this paper. This type of "creep stress" along the surface of the paper encourages the corona which will carbonize the surface until breakdown occurs. A breakdown or short between foils a and b increases the stress in the remaining sections of the capacitor, and failure of the entire capacitor

will soon follow. A creep-stress figure of 40V/mil includes a safety factor commensurate with a through-the-paper stress of 1kV/mil.

In the design which we propose, a variation of the staggered construction will be used which does not juxtapose the edges of adjacent foils. In the proposed design (Fig. 14) each foil edge is separated by a layer of paper from all other foil edges. This procedure allows a smaller offset of one foil with respect to its neighbor, provides a greater volume efficiency for a given length, and has superior edge protection.

The assembly of such a capacitor is accomplished by winding a single strip of paper sheet on a mandrel and inserting the single turns of foil sections, each one with an axial offset with respect to its predecessor.

Such capacitors have been constructed on cylindrical mandrels and tested at our laboratory. In the proposed case we will use an elongated (oval) cross section mandrel as shown in Fig. 15.

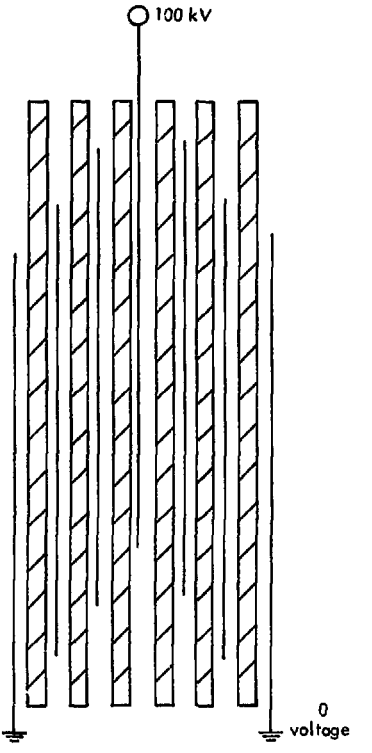

Fig. 14. Proposed high voltage capacitor with axially offset foils.

Capacitor-Section Design and Cooling Considerations

The previous section discussed the type of construction necessary to deal with the corona problem at the edges of the foils. In this section we examine actual figures and arrive at dimensional criteria for the construction of the basic capacitor sections, taking into account the necessities of adequate cooling.

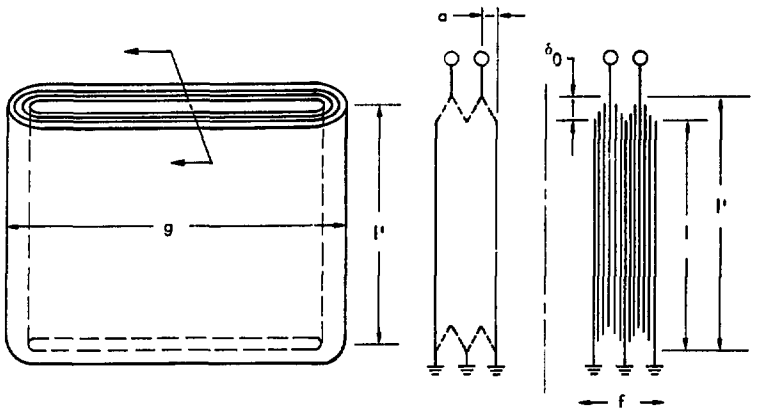

Fig. 15. High-voltage capacitor with vane cross section.

For ease of construction and maintenance, we are interested in building basic capacitor sections which store between 0.5% and 1% of the total energy. The geometry of such a section, which is shown in Fig. 15, is a plane rectangle where the foils are stacked in the plane. We will call this rectangle a "vane", whose cross section is shown at the right in Fig. 15.

The dimensions of the vane must be determined on the basis of voltage-holding capability and cooling requirements. The vane is constructed of a number of subsections. Each section of width "a" holds 100 kV and is made of m foils, each consisting of aluminum of thickness δ_{al} and oil-impregnated paper of thickness δ_p, so that

$$a = m(\delta_{al} + \delta_p).$$

At 1 kV per mil, and the choices of δ_{al} = 1 mil and δ_p = 5 mil, then m = 20 and "a" = 120 mil (i.e., 3 mm). The volume efficiency (η) is given by the ratio of the energy-storage volume over the total volume of the section. To hold the total voltage from the tip of the bottom foil to the top plate, an offset of δ_0 is proposed. This value is determined conservatively to be δ_0 = 100 kV/25V/mil = 4.in ≈ 10 cm. The length "ℓ" is assumed to be 1 m. Thus,

$$\eta = \frac{\delta_p}{\delta_{al} + \delta_p} \cdot \frac{\ell}{\ell + \delta_o}$$

$$= \frac{5}{1 + 5} \cdot \frac{1}{1 + 0.1} = 0.75$$

The first term accounts for the thickness of the aluminum and the second term accounts for the volume-offset losses. This volume efficiency does not include the mandrel volume or the volume surrounding the vanes. The volume is $2\ell'fg$. If an additional 15% width is used for cooling then the added volume is $2\ell'0.15fg$ and volume efficiency goes to $\frac{1}{1 + 0.15}\eta = 0.65$.

We now consider the minimum exposed surface area per section necessary for adequate cooling. Figure 16 shows experimentally-derived data which plot the temperature rise of the surface of an air-cooled oil-impregnated paper capacitor vs load resistance and wattage/square inch of capacitor surface area. A brief discussion of the origin of the temperature-rise dependence given in these curves is found in Appendix B.

To determine $R_{discharge}$ for our

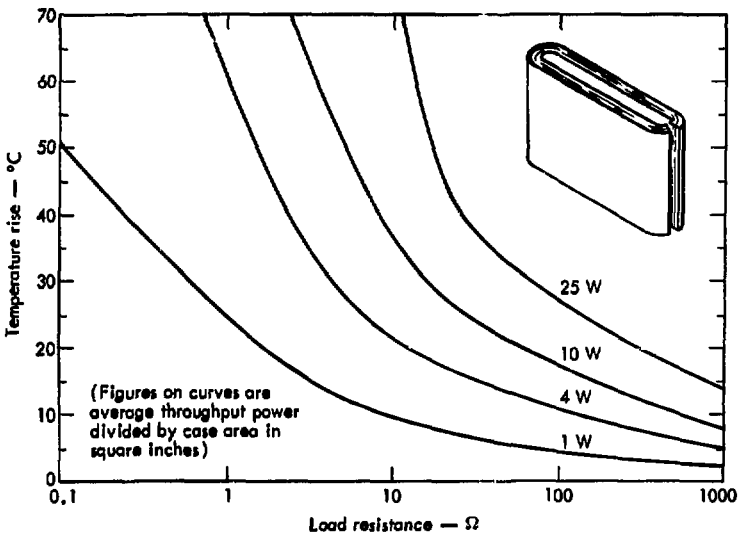

Fig. 16. Temperature rise vs external load resistance.

systems we can say that each vane carries a current of I_{total}/Z, where Z is the number of vanes. Hence, $R_{discharge}$ per vane is

$$R_{discharge} = \frac{VZ}{I_{total}}$$

$$\approx \frac{10^5}{10 \times 10^6} \cdot \frac{100}{} = 1 \ .$$

where

V = total voltage = 100 kV.

With selection of a temperature rise of 25°C as an appropriate figure and $R_{discharge} = 1\ \Omega$, the corresponding curve in Fig. 16 indicates a power of 1 watt/in^2. This figure of 1 watt/in^2 is a very conservative and safe choice because it is for an air-cooled capacitor can and we are using this figure for an oil-cooled capaciator vane. We will use 1 watt/in^2 = $(40)^2$ watt/m^2 as the effective power-to-area ratio, P/A, of our capacitor vane. Thus,

$$A = \frac{P}{(40)^2}\ m^2.$$

A vane is wound on a permanent hollow mandrel where cooling is provided on both the outside and the inside of the vane. The total volume per section in our geometry, excluding the mandrel and external space, is given by

$$V' = 2\ell' gf = \frac{V}{\eta} \ ,$$

where V is the energy-storage volume and η is the volume efficiency.

The net volume V per vane equals the energy per vane divided by the energy density. W is the total energy stored in the bank and Z is the number of vanes, so that

$$V = \frac{W}{Z} \cdot \frac{1}{\frac{1}{2}\epsilon E^2} \ .$$

The equation,

$$V' = 2\ell' gf = \frac{W}{Z} \cdot \frac{1}{\frac{1}{2}\epsilon E^2} \cdot \frac{1}{\eta}$$

relates the dimensions of the vanes to parameters which determine the volume, without yet having considered the space occupied by the hollow mandrel and the spacing between sections. To calculate the thickness of the vane "f" we determine the surface-to-volume ratio. The surface area available for cooling each vane is, from Fig. 15, equal to $4\ell' g$. The surface-to-volume ratio for our geometry then is:

$$\frac{A}{V'} = \frac{4\ell' g}{2\ell' gf} = \frac{2}{f} \text{ or } \frac{P}{(40)^2} \Big/ \frac{W}{\frac{1}{2}\epsilon E^2 \eta}.$$

Solving for f we obtain:

$$f = \frac{4W \cdot (40)^2}{\epsilon E^2 \eta P}.$$

Substituting Ws = P, where s is the number of shots per second, the vane width becomes:

$$f = \frac{4x(40)^2}{\varepsilon E^2 \eta s}.$$

For example, if we take s = 1,
$E = 40x10^6 \frac{V}{m}$, $\eta = 0.65$,
$\varepsilon = 5 \times \frac{10^{-9}}{36\pi}$ (for castor oil), then,

$$f = \frac{4x(40)^2 x36}{5x10^{-9}(40x10^6)^2 0.65}$$

$$= 0.14m = 14 \text{ cm}.$$

This is a conservative upper limit, from the point of view of cooling, to the thickness of the "roll" which forms the vane (see Fig. 15).

For a 1 MJ capacitor the net volume of dielectric is

$$\frac{W}{\frac{1}{2}\varepsilon E^2} = \frac{10^6 x36\pi}{\frac{1}{2}x5x10^{-9}(40x10^6)^2}$$

$$= 28.3 \text{ m}^3.$$

The volume occupied by the sections, without consideration of the hollow mandrel and spacing, is

$$(28.3/0.75 \text{ m}^3 = 37.7 \text{ m}^3 = 2\ell' \text{ gf}.$$

For example, if $\ell' = 1.2$ m, f = 0.14 m, and Z = 100, then

$$g = \frac{37.7}{2x100x0.14x1.2} = 1.125 \text{ m}.$$

The gross volume $V = \frac{28.3}{0.65} = 43.5 \text{ m}^3$. The number of foils within the dimension f is

$$\frac{14 \text{ cm}}{0.006x2.54\text{cm}} = 918$$

which we will round off at 920. The number of parallel subsections (see Fig. 15) is 920/20 = 46. We therefore, have 46 parallel subsections, each made of 20 foils in series. We know that the capacitance of the entire capacitor should be 200μF and we now check the capacitance of the capacitor we have just designed.

$$C = \frac{(\text{area})Z \times 46}{(\text{thickness})20}$$

$$= \frac{2\varepsilon\ell g x100x46/20}{5x10^{-3}x2.54\ 10^{-2}} = 198\ \mu F$$

where

thickness = 5mil = $5x10^{-3}x 2.54x10^{-2}$ in.
area = $2\ell g = 2x1.1x1.125$
Z = number of vanes = 100
ε (castor oil) = $\frac{5x10^{-9}}{36\pi}$
$\ell = 1.1$ m
g = 1.125 m

Inductance Considerations and Current Crowding

In order to make a capacitor so that it has a margin of safety in its performance, it is necessary not only to have it withstand the voltage but also for it to be able to carry the current without excessive heating of certain areas of the foils due to current crowding. "Current crowding" is a phenomenon which manifests itself as an unusually high current-density in certain regions of the

foil and in the electrical connections to the foil. This increased current density in the regions of current crowding causes large magnetic forces to act on the foils in conjunction with a greatly increased thermal stress due to the high I^2R losses in these regions. The combination of these two types of stresses can cause the capacitor to fail. To build a capacitor which is not subject to these difficulties we must examine the phenomenon of current crowding in some detail.

In Fig. 17 we can see schematically two foils connected in parallel to a bus. (Actually, there would be, typically, 40 parallel foils between each pair of foils shown.) The current flows on both sides of each of these connected foils but ends up flowing on the outside surfaces of the bus. The current flowing on the inside at the top of each foil has a magnetic field associated with it. This magnetic field has to penetrate the foil, or curl around the edge of the foil with its associated current, in order to end up on the outside surface. This problem is not so serious with only two foils connected to the bus, as depicted in Fig. 17, because the depth of penetration is typically equal to the foil thickness. But when as many as 40 foils are connected

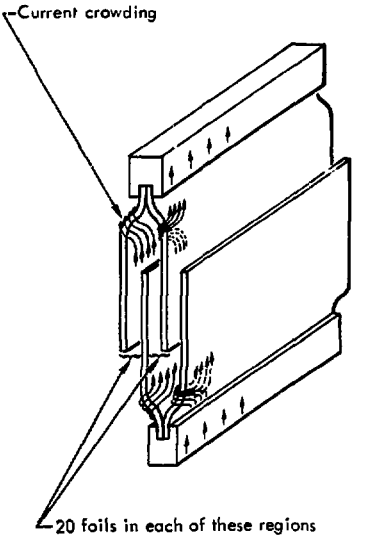

Fig. 17. Foil connections to bus in high-voltage capacitor.

to the bus, the current crowding would be severe because of the tortuous path which the inner currents must take to get to the external surface.

To solve the problem of current crowding, we propose to eliminate the multifoil connections, as diagrammed in Fig. 18. As shown in Fig. 18 (top), the gap in the foils allows the electromagnetic energy to exit through the dielectric material only, thus preventing current concentrations.

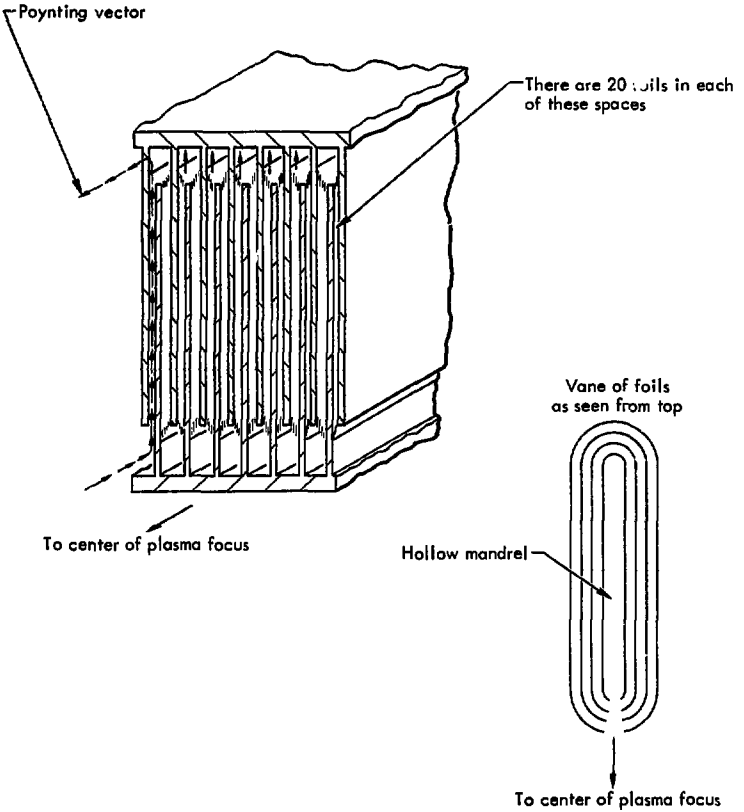

Fig. 18. Top and sectional views of typical high-voltage capacitor.

In Fig. 18, also, capacitor subsection foils are shown where every 20th foil is connected either to the top plate or the bottom plate. The direction of the Poynting vector is indicated by a dashed line. Note how the Poynting vector proceeds directly from the dielectric region to the load region without obstruction. Every twentieth foil (which is connected alternately to the top or bottom plate) will be somewhat heavier than the others--about 4 mils thick (about 0.1mm) instead of 1 mil. to provide physically stronger connections. The length and thickness of these connecting foils could be chosen to serve as protecting fuses. If part of the bank tries to dump into one shorted capacitor, these foils will heat up and thereby increase their resistance to the point where they become the predominant load, thus absorbing the energy in a non-destructive way.

As we have discussed in the introduction, the 16-fold volume increase necessary to reduce voltage stress puts severe limitations on our ability to design the entire bank for low inductance. In the following paragraphs, we develop a bank configuration with very low inductance.

We now determine the inductance that the capacitor presents to the discharge current. Figure 19 is a schematic representation of the plasma-focus capacitor, switches, parallel-plate transmission line and the plasma focus itself.

We first compute the inductance associated with the entire volume occupied by the capacitor bank in the absence of the capacitor vanes. This will give us the extreme upper limit for the bank itself. Assume a path for the current I, flowing down at r_o and up at r_3. The inductance, L_A, will be due to the annular volume enclosed by $(\pi r_3^2 - \pi r_o^2)$. In the region $r_o<r<r_3$, the magnetic field H_θ due to the current I is

$$B = \mu_o \, I/2\pi r \ T$$

where

$$\mu_o = 4\pi \times 10^{-7} \ h/m.$$

The magnetic flux $\phi = \int_{r_o}^{r_3} B\ell dr$

$$= \frac{\mu_o I \ell}{2\pi} \int_{r_o}^{r_3} \frac{dr}{r} = \frac{\mu_o I \ell}{2\pi} \ell n \frac{r_3}{r_o}$$

$$\phi = 2\times10^{-7} I \ell \ \ell n \frac{r_3}{r_o} \ Wb.$$

Therefore,

$$L_A = \frac{\phi}{I} = 2 \times 10^{-7} \ \ell \ \ell n \frac{r_3}{r_o} \ H \ .$$

Now we compute the inductance associated with the same volume, where the current I flows down at r_o (in Fig. 19) but flows back up along

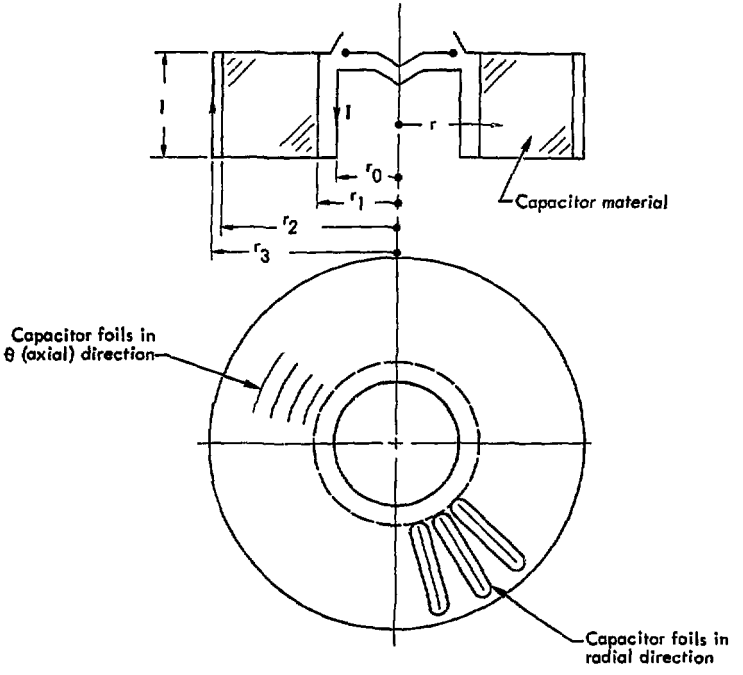

Fig. 19. Schematic representation of plasma-focus capacitor, switches, parallel-plate transmission line and plasma focus itself.

the entire radius ($r_o<r<r_3$) with a uniform current density.

This computation will give us an estimate of the inductance associated with the volume filled with capacitor foils but allowing mutual flux to couple all currents.

That is,

$$j(r) = \frac{-I}{\pi(r_3^2-r_o^2)} .$$

Then

$$H\cdot 2\pi r = I - j\int_o^r 2\pi r dr$$

$$= I - j\pi(r^2-r_o^2)$$

and

$$H = \frac{I}{2\pi r}\left(1 - \frac{r^2 - r_o^2}{r_3^2 - r_o^2}\right) = \frac{I}{2\pi r}\left(\frac{r_3^2 - r^2}{r_3^2 - r_o^2}\right) = H_B .$$

The inductance L_B associated with this current configuration,

where $\phi = \int_{r_o}^{r_3} \mu_o H \ell \, dr$,

is,

$$L_B = 2 \times 10^{-7} \ell \left[\left(\frac{r_2^2}{r_3^2 - r_o^2}\right) \ell n \frac{r_3}{r_o} - 1/2\right] H .$$

Now let us compare L_B and L_A:

$$\frac{L_B}{L_A} = \frac{r_3^2}{r_3^2 - r_o^2} - \frac{1}{\ell n \frac{r_3^2}{r_o^2}} = \frac{\left(\frac{r_2}{r_o}\right)^2}{\left(\frac{r_2}{r_o}\right)^2 - 1} - \frac{1}{\ell n \left(\frac{r_2}{r_o}\right)^2} .$$

Representative values for the bank's volume are: volume = 43.5 m^3, $r_2 - r_1 = 1.125$ m, and $\ell' = 1.2$ m. Then,

$$\frac{43.5}{\ell'} = \pi\left(r_2^2 - r_1^2\right) = \pi\left(r_2 - r_1\right)\left(r_2 + r_1\right)$$

$$r_2 + r_1 = \frac{36.25}{\pi 1.125} = 10.25$$

$$= 1.125 + r_1 + r_1$$

$$2r_1 = 9.13$$

$$r_1 = 4.56 \text{ m}$$

and

$$r_2 = 5.7 \text{ m}$$

Thus, for $r_o \approx r_1$ and $r_3 \approx r_2$ we have

$$\frac{r_3}{r_o} = \frac{5.7}{4.56} = 1.25 \text{ and } \left(\frac{r_3}{r_o}\right)^2 = 1.55.$$

Therefore,

$$\frac{L_B}{L_A} = \frac{1.55}{0.55} - \frac{1}{\ln 1.55} = 2.8 - 2.28 = 0.52.$$

Thus the return of the current I with a uniform current density throughout the volume of the capacitor reduces the inductance to about 0.52 of L_A.

The values of H_A and H_B as a function of radius (r) are plotted in Fig. 20. If the foils of the capacitor are run in the θ direction, as shown in Fig. 19, the value of $H_\theta(r)$ will be as shown by H_C in Fig. 20. The corresponding inductance L_C will be very similar to L_B.

If, however, the foils of the capacitor run predominantly in the radial direction, as shown in Fig. 19, the foils are perpendicular to H_θ, the field produced by the load current. It is the field H_θ which

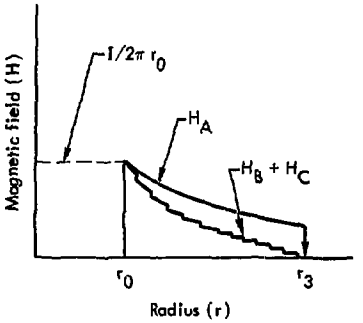

Fig. 20. H_A, H_B and H_C vs radius.

the previous geometries have failed to reduce. To a first approximation (a thorough field solution is given in Appendix A), since the dc field solution requires that H run perpendicular to all the 100,000-odd foils, i.e dc solution does not apply to the ac case. For the case in which the foils run in the θ direction, the dc and ac field solutions are similar and the flux occupies the entire foil region. To a first approximation for the radially oriented foils, the magnetic flux is completely excluded from the foil region. Of course, H_θ exists in the region between r_0 and r_1 and the region between r_2 and r_3 and some of this field does penetrate between the foils, as shown in Appendix A. The inductances in the regions r_0 to r_1 and r_2 to r_3, are designated L_1 and L_3 respectively.

From Appendix A

$$L_1 = 0.485 \times 10^{-7} \ell' \ln \frac{r_1}{r_0} \text{ H}$$

$$L_3 = 0.485 \times 10^{-7} \ell' \ln \frac{r_3}{r_2} \text{ H},$$

and the vane region inductance is

$$L_2 = \frac{2.46 \times 10^{-7} \ell'}{2N} \text{ H},$$

where

2N = number of vanes.

For the proposed radial packing (Fig. 21) the radius r_1, must allow 100 vanes around the circumference. Thus, since the width of each vane is 30 cm $\{2 \times (14 + 1)\}$ the circumference must be 30 m.

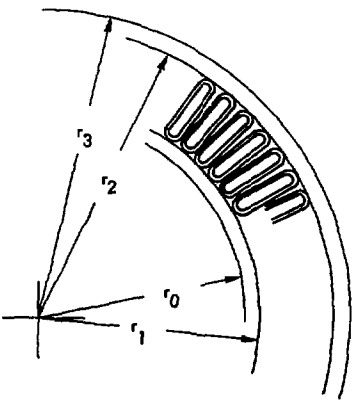

Fig. 21. Radial vs axial foil placement in high-voltage capacitor.

Therefore

$$r_1 = \frac{30}{2\pi} = 4.77 \text{ m.}$$

The minimum r_1 from volume considerations is 4.56 m. We will select a design value of 4.8 m for r_0 and a value of 6 m for r_3. Thus,

$$L_A = 2 \times 10^{-7} \ell' \ln \frac{r_3}{r_0} = 2 \times 10^{-7} \times 1.2 \cdot \ln \frac{6}{4.8} = 53 \text{ nH}$$

$$L_B = 0.52 \, L_A = 28 \text{ nH}$$

$$L_C \approx L_B = 28 \text{ nH}$$

$$L_1 = 48.5 \times 10^{-9} \times 1.2 \ln \frac{4.85}{4.8} = 0.48 \text{ nH.}$$

and

$$L_3 = 48.5 \times 10^{-9} \times 1.2 \ln \frac{6}{5.965} = 0.34 \text{ nH.}$$

To calculate L_2 we have to choose the proper number of foils. The total number of foils is 20x46x100 = 92 000. However, we have 200 gaps 1 cm wide between the sections and in the mandrel. For an extremely conservative estimate let us decrease the density of foils to provide 1 cm gaps between each 2 foils. For a 30 m circumference with gaps of 1 cm the number of foils (2N) equals 3000. That is,

$$L_2 = \frac{2.46 \times 10^{-7} \times 1.2}{3000} = 9.8 \times 10^{-11} \text{ H.}$$

Thus the total inductance of the bank is $L_1 + L_2 + L_3 \approx 0.9$ nH. This represents a small contribution to the system total.

The inductance of the transmission line, the switches, and the stepped inductor must be added in. For a 0.3 cm spacing between the parallel-plate transmission line plates, the inductance of the transmission line is $0.3 \times 2 \times \ell n \frac{4.8}{0.5} = 1.36$ nh.

The switch inductance will be calculated on the basis of using 2 in diameter SCR chips 0.5-mm thick. Thus,

$$L/\text{wafer} = 0.1 \times 10^{-9} \left(0.5 + \ln \frac{3.54}{2.54}\right) = 8.3 \times 10^{-11} \text{ H/wafer.}$$

Since there are 100 wafers in series and 100 switches in parallel the total switch inductance is 8.3×10^{-11} H.

The inductance of the stepped inductor when saturated is:

$$L = \frac{\mu_o}{2\pi} \times 2 \times 10^{-2} \ln \frac{167}{100} = 2 \text{ nH .}$$

The total inductance of the bank, switch, transmission line, and stepped inductor (saturated) is:

$$L_{Total} = 0.9 \text{ nH} + 1.36 \text{ nH} + 0.1 \text{ nH} + 2.05 \text{ nH} = 4.41 \text{ nH.}$$

We propose to make a small-scale electrical mock up of the capacitor bank and check the inductance at the appropriate frequency to verify our inductance calculations for the capacitor.

POWER SOURCE AND CHARGING CIRCUIT

The pulsed-plasma-focus neutron and radiation facility will be operated at one pulse per second at an average power expenditure of 1 MW. It should be feasible to purchase this extra power from local utilities.

Considering the energy crisis, the extra lines to be built, the large interference with normal utility operations and the buffer costs, it would be more advantageous to have our own stationary power source. A convenient source would be a compact gas turbine generator set, similar to the type power companies use for peak energy shaving. We therefore propose a gas turbine stationary energy source charging an intermediate capacitor bank, as shown in Fig. 22.

Waveforms showing the timing of this circuit (on a logarithmic time scale) are shown in Fig. 22. In this circuit we take advantage of the unidirectional properties of the SCR switch which stops the ringing of the bank with the SFG load after 1/2 cycle. Thus all the energy not consumed in the focus ends up in the bank with opposite polarity. Typically this energy amounts to half of the initial bank energy. In the circuit of Fig. 22 C_B in series with C_s and L can ring only 1/2 cycle because of diode D. If the values are properly chosen, at the end of the 1/2 cycle C_B will be charged to the initial required voltage and be ready to fire, and C_s will be completely discharged. If this ringing is performed in 10 msec, then the charging current to C_B will be a few thousand amps, which is reasonably low. Typical parameters, assuming 50% energy loss in the focus, are shown in Fig. 22. For this case C_s is 1166 μF and V_s is 29.3 kV.

SWITCHING

The switch requirements for the SFG energy source are relatively easy to meet individually, but collectively they are beyond the current state of the art.

The general switch requirements are to hold off 100 kV in the forward direction and conduct 10^7 A for 3-4 μs after closing. The switch must be able to operate at a repetition rate of at least one pulse per second for approximately 10^7 shots. Finally, the switch inductance should not be

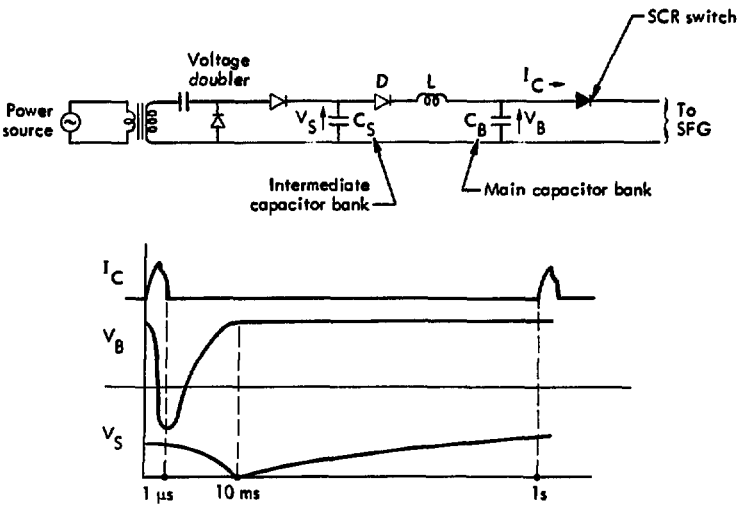

Fig. 22. Power source simplified schematic and timing diagram.

larger than a fraction of 1 nH.

The peak power requirement in itself is not difficult to meet. A single high-pressure spark gap can block 100 kV and conduct 100 kA for a few microseconds and have an inductance below 100 nH so that the desired requirement can be met by 100 such parallel switches. However, the life of these switches cannot be stretched much above 10^4 shots (3 hours). Electrode erosion and the deposition of electrode material on the insulating walls of the switch are the cause for the limited life expectancy. A further limitation is imposed by the high average power requirement ($\sim$ 1 MW) that the switch has to transfer. Typically, these switches absorb between 0.1 and 1% of the energy they transfer. Thus, as much as 10 kW of heat has to be removed, thus imposing a further limitation on the use of these switches in the design of the capacitor bank.

We have investigated all potential candidates for this switching application such as the vacuum switch, ignitrons, thyratrons,

high-pressure spark gaps, liquid (oil and water) dielectric gaps, solid-dielectric switches, and solid-state switches.

Thyratrons and ignitrons are ruled out because of power, inductance and longevity limitations.

Short life, high inductance, and low average power rule out the vacuum spark-gaps, high-pressure spark gaps, and the solid dielectric switches. It appears that the only useful candidates are the liquid-dielectric and the solid-state switches.

A liquid-dielectric switch is shown in Fig. 23. The close spacings permitted by the immersion of the assembly in transformer oil and the insulating and heat-exchange properties of the oil make the switch relatively small and compact. The liquid dielectric is "self healing" and the transformer oil will be pumped continuously through a filter to remove any contamination which would otherwise build up. Large rotatable electrodes provide ample surface area for erosion and thus assure long life.

The most promising switch, however, is the solid state device. A very important advantage is that semiconductor devices have practically limitless life. Currently-manufactured silicon controlled rectifiers (SCR's), in particular, are capable of holding off 1000 to 2000 volts per unit, with current-carrying ability, in the sinusoidal steady state, of approximately 1000 A. This power level is too small for our application. However, in the turn-on regime of 10^{-4} s, a wafer about 0.5-mm thick and 2 inches in diameter can carry 100,000 to 200,000 A for a short period of time. These devices are still not satisfactory for our requirements because the turn-on time is much too slow.

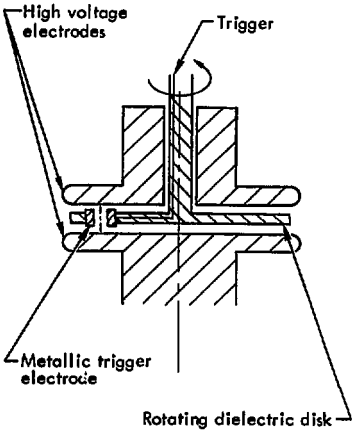

Note: Switch is immersed in oil

Fig. 23. Oil-immersed rotating-electrode high-energy switch.

Recently, however, great advances have been made in turn-on-time characteristics. In particular, development by the Westinghouse Research Laboratories* has shown that direct optical triggering makes the SCR a prime candidate for our application. In their method of triggering, a laser beam, matched to the silicon wafer band gap, illuminates the wafer thus generating electron-hole pairs necessary for conduction.

To date, a 40,000 A/μs current rise has been achieved. This rate is due to external-circuitry limitation rather than device limitation. Thus such a device will provide 100,000 A in 3 μs, the time necessary for the discharge of the capacitor bank into the plasma focus device. Thus, 50 to 100 such units in parallel will carry the total 5 to 10 MA necessary to energize the plasma-focus device. Since the voltage-holding capability of the wafer is only 1 to 2 kV, we need, again, 50 to 100 such units in series. The laser-beam initiated turn-on time has been successfully demonstrated for such large series arrays. Since the turn-on time is practically instantaneous, there is no avalanche failure. Thus the total number of wafers needed for our switch is five- to ten-thousand wafers.

The inductance of these wafers is extremely small. This is because the current flows through the total area of the wafer. Consequently, the current path occupies a large cross-sectional area. Such an array of 10,000 wafers will be arranged to be part of the transmission-line geometry so as to minimize the self inductance. In fact, we can make this inductance almost negligible. See Fig. 24.

For these 10,000 units we need approximately 10 to 100 J of laser power delivered within 20 ns. This can be easily achieved with a single laser oscillator and ten 10-joule amplifiers. To date, the cost of the SCR wafers is in the region of $100 each. This is with the purchase of single units. Thus the cost of the silicon wafers alone would be in the neighborhood of $1,000,000. If we include the laser and mounting costs and the large-quantity purchase price reductions for the silicon, we can estimate the switch price between one and two million dollars.

*Reference to a company or product name does not imply approval or recommendation of the company or product by the University of California or the U.S. Energy Research & Development Administration to the exclusion of others that may be suitable.

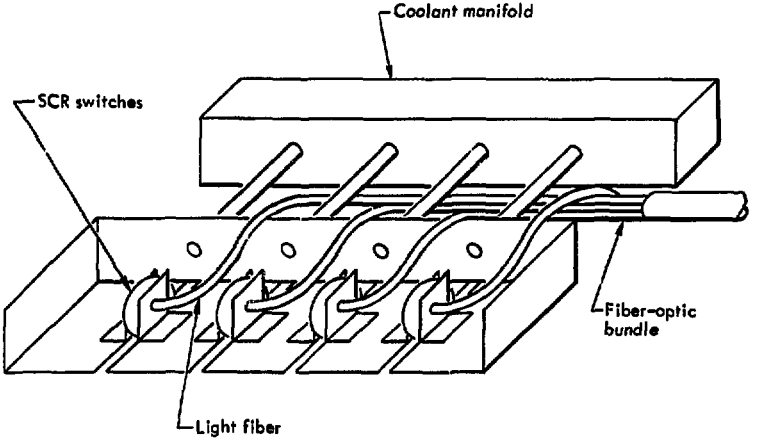

Fig. 24. Construction detail of optically triggered solid-state switch.

For comparison with conventional switches (high-pressure spark gaps) Table 3 indicates that even with only 10 million discharges for the SCR system, it is between a factor of 50 to 100 times cheaper than a high-pressure spark gap.

Thus, the light-activated SCR is, by far, the most logical choice for our applications. Hence, we have initiated negotiation with Westinghouse on the development of such a switch tailored to our application, and a proposal has been submitted by them to develop a prototype. As shown in the previous section, a 10^4 wafer unit having a total inductance of less than 0.1 nH is more than adequate for the job.

Table 3. Inductance per unit

	V/unit	I/unit	Power/ unit	Induct- ance	No. of units needed for 10^{12} watts	Shots/ unit	No. of units needed for 10^{12} watts and 10^{7} shots	Cost per unit ($)	Total cost ($)
High Pressure spark gap	10^{5}	10^{5}	10^{10}	100 nH	10^{2}	10^{4}	10^{5}	1000	10^{8}
SCR	10^{3}	10^{5}	10^{8}	.001 nH	10^{4}	10^{7}_{+}	10^{4}	200	$2x10^{6}$

Research and Development

SHORT RANGE DEVELOPMENT

Listed below are the technical problems which must be solved to assure reliable, continuous operation of a fusion reactor simulator capable of delivering 10^{15} DT neutrons per second.

High Voltage Operation of the SFG

It is clear that the optimum conditions for formation of the current sheet in plasma-focus devices are quite different from the optimum conditions for driving the current sheet after it is formed. It is known from experiments and theory that a too rapid current increase during current-sheet formation results in an instability which prevents formation of a uniform plasma. Conversely, a rapid current rise is desirable in order to obtain a high peak current. To meet these requirements we have proposed a stepped-inductance system which provides a high initial external inductance and low inductance after the current sheet is formed. This system should permit the use of smaller guns, higher bank voltage and higher peak current. As an initial step we suggest the installation of 80 to 100 kV capacitors on our present SFG device as soon as possible in order to gain early operational experience with a high voltage system. We also propose

to start life-testing components of the repetitively pulsed 1 MJ, 1 pps, capacitor bank at voltages from 100 kV to 400 kV, to accumulate experience on the life of these capacitors at higher voltages.

Switch Development

The development of light-activated silicon switches is now in progress at Westinghouse Research Labs. The operation of large series-parallel arrays of these switches must be proved feasible.

Concurrently, the development of a liquid-dielectric switch must be undertaken to provide a suitable alternative to the light-activated silicon switches.

Long-Life Capacitor Bank

Component development and testing for the proposed capacitor bank must be undertaken with careful attention given to the radiation problem. An important aspect of the radiation problem is the determination of capacitor shielding requirements with respect to longevity.

Electrode Erosion

Electrode erosion in the plasma focus is cumulative. Thus geometrical electrode arrangement and techniques of feeding new electrode material must be developed and tested to alleviate the erosion problem. The solution reached must not cause degradation of the focus performance.

Insulator Development

The insulator in the plasma focus provides the initial breakdown surface for the plasma sheet. To provide adequate lift-off of the plasma sheet and minimize restrike problems the insulator must maintain its integrity over many shots. Until now, Pyrex glass has been the choice of most investigators. However, it seems quite likely that for a repetitive by pulsed application a more refractory insulator will have to be developed.

LONG RANGE RESEARCH

In addition to the above short-range development plan, it is also proposed that more fundamental research be initiated to increase neutron- and plasma-wind yield. For several years LLL has studied fundamental changes in plasma-focus operation which are aimed at increasing efficiency and which have the ultimate goal of achieving break-even fusion. Obviously, it is not necessary to achieve breakeven fusion to increase greatly the utility of the plasma focus. We believe we can, with higher energy systems, achieve

approximately 10^{17} DT neutrons in short pulses once we improve our understanding of the neutron-producing mechanisms of the DPF.

The nature of the process which energizes deutrons so that they produce neutrons in the plasma focus is certainly not understood or agreed upon by all plasma-focus investigators. In the calculations of the scaling of neutron yield with current in the plasma focus, a Bennett relation, $I = 200\ NkT$, is usually assumed. It is also assumed for the most part, that the plasma is a thermal ensemble which has been heated by adiabatic compression of its cylindrical shape to a small radius. However, the anisotropy of the neutron energy and the appearance, reported by several observers, of two neutron pulses approximately 100 to 200 ns wide, spaced by 300 ns, makes this simple adiabatic-compression picture untenable.

Investigators at Stevens Institute of Technology and the Instituto Electrotecnico Nazionale in Turin, working with small plasma-focus machines, have shown that the x-rays come from localized "apple-core"-shaped volumes as small as 50 μm in diameter. The number of short-duration neutron and x-ray pulses (approximately 10 ns in duration) agrees on the average with the number of localized x-ray spots. The short-duration neutron pulses are obtained only with the neutron scintillator very close to the plasma focus (approximately 15 cm). It appears that we can draw a fairly firm conclusion that the x-rays and neutrons in these small machines come from localized concentrations of plasma which live for about 10 ns each. As the neutron and x-ray production in these small plasma-focus machines increases with increased voltage on the machine, however, the question remains whether the increased neutron and x-ray production is due to a greater multiplicity of localized-concentrated sources or to a greater strength of each source.

Acknowledgments

Thanks are due to H. M. Graham for contributing his valuable knowledge and experience of capacitors in the development of this design. Also, the authors wish to express their thanks to R. M. Bevensee for his work in preparing Appendix A on stored magnetic energy in a circular vane structure.

References

1. W.H. Bostick, V. Nardi and W. Prior, J. Plasma Phys. 8, 7 (1972).
2. R.F. Post, Physics Today (April, 1973).
3. Proc. Annu. Mtg. Div. Plasma Phys. of Am. Phys. Soc., 15th, Section 4H, in Bull. Am. Phys. Soc. (October, 1973), p 1318.
4. H. Rapp, Phys. Lett, 43A, 420 (1973).
5. V.S. Imshennik, N.V. Filippov and T.I. Filippov, Nucl. Fusion, 13, 929 (1973).
6. L. Michel, K.H. Schönbach and H. Fisher, Appl. Phys. Lett, 24 (2), 57 (1974).
7. D.A. Freiwald and J.N. Downing, A Survey of a 210-kJ Dense Plasma Focus (DPF-6), Los Alamos Scientific Laboratory, Rept. LA-5635-MS (1974).
8. V. Nardi, Physical Rev. Lett. 25, 11 (1970).
9. V. Nardi, Proc. Europ. Conf. on Controlled Fusion and Plas. Phys. 5th (Grenoble) paper 163, E5 (1972).
10. D.R. Wells and J.N. Norwood, Phys. Fluids 7, 1582 (1968).
11. D.R. Wells, J. Plasma Phys. 4, 645 (1970).
12. D.R. Wells, J. Plasma Phys. 3, 21 (1969).
13. W. Bostick, V. Nardi, W. Prior and F. Rodriquez-Trelles, "On the Nature of Highly Localized X-Ray Sources in the Plasma Focus," in Proc. Topical Conf. on Pulsed High-Beta Plasmas, 2nd, (Garching, 1972), p 155.
14. I.F. Belyaeva and N.V. Filippov, Nuclear Fusion 13, 881 (1973).
15. H. Conrads, P. Cloth, M. Demmler and R. Hecker, Phys. Fluids 15 (1), 209 (1972).
16. J.H.Lee and D.R. McFarland, Bull. Am. Phys. Soc. 17, 1023 (1972).
17. W.H. Bostick, V. Nardi and W. Prior, Annals New York Acad. Sci. 251, 2 (1975).

Appendix A

Estimation of Internal Stored Magnetic Energy in a Circular Vane Structure

Cross-sectional and partial top views of the vane structure are shown in Fig. A-1. This structure will be examined as a parallel RLC circuit oscillating as a high Q circuit after the switches are closed between the vanes and center post. Each vane consists of numerous parallel plates connected alternately to the top and bottom of the structure and is charged initially before the switches are closed. Let the total capacity of all the vanes in parallel be C_T. When the switches are closed, the vanes discharge through the center post and the outer guard ring (which may be connected or not, along the dashed surface in Fig. A-1; the difference is a negligible fringing capacitance) and they dissipate energy in the walls. The stored magnetic energy between the vanes and in the inner and outer gaps represents an inductance L_T in parallel with C_T and the effective conductance G_T. As the vanes discharge, the total current through the center post varies essentially as $\exp(-G_T t/C_T) \cos \omega_o t$, $t \geq 0$.

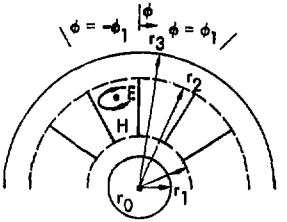

Top view, showing labeling of dimensions.

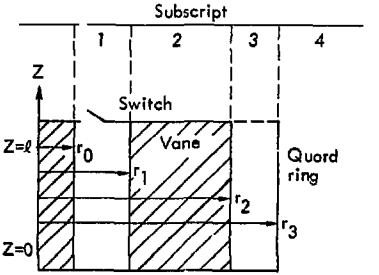

Cross-section through o vane.

Fig. A-1. Circular vane structure.

We shall estimate the relative amounts of stored magnetic energy in the gaps and in the vane region $r_1 \le r \le r_2$. To do this, we shall make the practical assumption that C_T is so large that the resonant wavelength λ_0 is far larger than the largest dimension of the system.

To determine the various contributions to inductance L_T we neglect the variation with Z of the primary field quantities and assume $\partial/\partial\phi = 0$ in the gaps, where $r_0 \le r \le r_1$, $r_2 \le r \le r_3$. Maxwell's equations then determine the primary field quantities within the inner gap (subscript 1) as

$$E_{Z1} = A_1\left[J_0(kr) - \frac{J_0(kr_0)}{Y_0(kr_0)}\,Y_0(kr)\right] \qquad (1a)$$

$$H_{\phi 1} = jA_1\left(\frac{\varepsilon}{\mu}\right)^{1/2}\left[J_1(kr) - \frac{J_0(kr_0)}{Y_0(kr_0)}\,Y_1(kr)\right] \qquad (1b)$$

$r_0 \le r \le r_1$, all ϕ

where $E_{Z1} \equiv 0$ at r_0, and $k = \omega_0/c = 2\pi/\lambda_0$.

The magnetic field vector $\bar{H}$ within one of the vane gaps behaves qualitatively as shown in Fig. A-1; it consists of H_r- and H_ϕ-components. We seek a simple solution to Maxwell's equations at frequency ω_0 in the vane region $r_1 \le r \le r_2$, $0 \le \phi \le \phi_1$ so that $\bar{H}$ and the implied E_Z will satisfy the boundary condition of $E_Z = 0$ at $\phi = 0$, ϕ_1. E_Z satisfies the wave equation, and in cylindrical coordinates with $\partial/\partial Z = 0$ this equation defines the Bessell function J_N or Neumann function Y_N, with $N \equiv \pi/\phi_1$. So in that vane region, (subscript 2)

$$E_{Z2} = [A_2Y_N(kr) + A_3J_N(kr)]\sin N\phi \qquad (2a)$$

$$H_{r2} = \frac{1}{\omega\mu}\,\frac{N}{r}\,[A_2Y_N(kr) + A_3J_N(kr)]\cos N\phi \qquad (2b)$$

$$H_{\phi 2} = -j\left(\frac{\varepsilon}{\mu}\right)^{1/2}[A_2Y_N(kr) + A_3J_N(kr)]\sin N\phi \qquad (2c)$$

where

$\equiv \partial/\partial(kr)$, $J_N(kr) \simeq \frac{1}{N!}\left(\frac{kr}{2}\right)^N$,

and $Y_N(kr) \simeq -\frac{(N-1)!}{\pi}\left(\frac{2}{kr}\right)^N$

for the assumed $kr = 2\pi r/\lambda_0 << 1$.

In the outer gap (subscript 3) we have field variations like those of the inner gap,

$$E_{z3} = A_4\left[J_0(kr) - \frac{J_0(kr_3)}{Y_0(kr_3)}\,Y_0(kr)\right] \qquad (3a)$$

$$H_{\phi 3} = jA_4\left(\frac{\varepsilon}{\mu}\right)^{1/2}\left[J_1(kr) - \frac{J_0(kr_3)}{Y_0(kr_3)}\,Y_1(kr)\right] \qquad (3b)$$

$$r_2 \le r \le r_3, \quad \text{all } \phi$$

which constrain $E_{z3}(r_3) \equiv 0$.

Since N is, in practice, so large, i.e., >10, (note that the number of vanes is 2N) the Y_N- and Y'_N-components of the vane-gap field predominate at r_1 while the J_N and J_N-components completely dominate at r_2. Hence we can match boundary conditions and determine A_1---A_4 in terms of a single vane current I_V as reference because the inner vane region $r \lesssim 1/2(r_1 + r_2)$ is effectively "decoupled" from the outer region $r \gtrsim 1/2(r_1 + r_2)$.

Assuming $I_V/2$ flows through each half of a vane we have, from the fact that $H_r2(r,\phi{=}0)$ of Eq. 2b equals $J_V/2$ at each point,

$$\frac{j}{\omega\mu}\,NA_2\int_{r_1}^{r_2}\frac{1}{r}\,Y_N(kr)\,dr \simeq \frac{1}{2}\,I_V \qquad (4a)$$

which determines A_2 in terms of I_V; and also

$$\frac{j}{\omega\mu}\,NA_3\int_{r_1}^{r_2}\frac{1}{r}\,J_N(kr)\,dr \simeq \frac{1}{2}\,I_V \qquad (4b)$$

which determines A_3. The result is these expressions for the $\bar{H}$-field in each vane-gap region,

$$H_{r2}(r,\phi) = I_V\frac{N}{2r}\left[\left(\frac{r_1}{r}\right)^N + \left(\frac{r}{r_2}\right)^N\right]\cos N\phi \qquad (5a)$$

$$H_{\phi 2}(r,\phi) = I_V\frac{N}{2r}\left[\left(\frac{r_1}{r}\right)^N - \left(\frac{r}{r_2}\right)^N\right]\sin N\phi \qquad (5b)$$

$$r_1 \le r \le r_2, \quad 0 \le \phi \le \phi_1$$

To evaluate amplitude A_1 of the inner-gap field, (Eq. 1), we will equate the sin Nϕ- component of $H_{\phi 1}$ at r_1 to that spacial component of $H_{\phi 2}$ in the vane-gaps at r_1. This is the first step in a procedure of evaluating a complete set of mode amplitudes in the vane-gap region in terms of the

amplitudes of another set in the inner gap region by multiplying successively by sin Nφ, sin 3Nφ,... and integrating from 0 to ϕ_1. The result is, using Eq. 5b at r_1,

$$\int_0^{\phi_1} H_{\phi 1}(r_1)\sin N\phi \, d\phi = I_V \frac{N}{2r_1} \int_0^{\phi_1} \sin^2 N\phi \, d\phi \quad (6a)$$

which yields

$$H_{\phi 1}(r_1), \text{ uniform in } \phi \ , = I_V \frac{\pi N}{8r_1} \ . \quad (6b)$$

Knowing that $H_{\phi 1}$ varies with r as in Eq. 1b and has the value (Eq. 6b) at $r=r_1$ enables us to write, for the inner gap region

$$H_{\phi 1}(r) = I_V \frac{\pi N}{8r_1} \frac{J_1(kr) - R_1 Y_1(kr)}{J_1(kr_1) - R_1 Y_1(kr_1)} \ , \quad r_0 \le r \le r_1 \quad (7)$$

$$R_1 \equiv J_0(kr_0)/Y_0(kr_0) \ .$$

By proceeding similarly to equate sin Nφ- components of H_ϕ on the $r = r_2$ surface we obtain $H_{\phi 3}(r)$ in the outer gap region in terms of I_V as

$$H_{\phi 3}(r) = -I_V \frac{\pi N}{8r_2} \frac{J_1(kr) - R_3 Y_1(kr)}{J_1(kr_2) - R_3 Y_1(kr_2)} \ , \quad r_2 \le r \le r_3 \quad (8)$$

$$R_3 \equiv J_0(kr_3)/Y_0(kr_3) \ .$$

We may now proceed to compare magnetic stored energies. With $Y_0(kr) = -\frac{2}{\pi} \ln \frac{2}{\gamma kr}$, $\gamma = 1.781$, $H_{\phi 1}$ and $H_{\phi 3}$ simplify because $kr \ll 1$:

$$H_{\phi 1}(r) \simeq I_V \frac{\pi N}{8r} \ , \quad r_0 \le r \le r_1 \quad (9a)$$

$$H_{\phi 3}(r) \simeq - I_V \frac{\pi N}{8r} \ , \quad r_2 \le r \le r_3 \quad (9b)$$

and we find for the time average magnetic stored energies in the gaps, $W = \frac{1}{4} \mu_0 \int H^2 \, dv$,

$$W_1 = \mu_0 I_V^2 \frac{\pi^2 N^2}{256} \ln \frac{r_1}{r_0} \ , \text{ inner gap} \quad (10a)$$

$$W_3 = \mu_0 I_V^2 \frac{\pi^2 N^2}{256} \ln \frac{r_3}{r_2} \ , \text{ outer gap} \quad (10b)$$

while the stored magnetic energy w_2 in one vane-gap region is

$$w_2 = \frac{1}{4} \mu_0 \int_{r_1}^{r_2} r\,dr \int_{\phi=0}^{\phi_1} d\phi \, [H_{r2}^2 + H_{\phi 2}^2] = \mu_0 \frac{I_V^2 \pi}{64} \ . \quad (11a)$$

The magnetic energy in the entire vane region is 2N times this or

$$W_2 = \mu_0 I_V^2 \frac{\pi N}{32} , \quad r_1 \le r \le r_2 . \qquad (11b)$$

The magnetic energy stored in the vane region will be negligible compared to that in the inner gap if

$$W_2/W_1 = \frac{8}{\pi N \ln \frac{r_1}{r_0}} << 1 , \qquad (12a)$$

and W_2 will be small relative to the energy in the outer gap if

$$W_2/W_3 = \frac{8}{\pi N \ln \frac{r_3}{r_2}} << 1 . \qquad (12b)$$

It is interesting to note that the inductances L_1 and L_3 associated with the inner and outer gaps, defined with respect to total vane current $2N I_V$:

$$W_1 = \tfrac{1}{4} L_1 (2N I_V)^2 , \; W_3 = \tfrac{1}{4} L_3 (2N I_V)^2 \qquad (13)$$

evaluate as (MKS units)

$$L_1 = 0.485 \times 10^{-7} \ln \frac{r_1}{r_0} \qquad (14a)$$

$$L_3 = 0.485 \times 10^{-7} \ln \frac{r_3}{r_2} , \qquad (14b)$$

whereas we would expect these answers but with coefficients of 0.500 in the limit of $N = \infty$. This is because each gap is then like an ordinary coaxial line with an inductance per unit axial length of 2×10^{-7}, but the magnetic field in each gap is <u>half</u> the total amount in the vanes, hence the inductance is one quarter the ordinary coaxial line value.

If the outer gap were absent ($r_2 = r_3$) the formulas would change as follows: $H_{\phi 1}(r)$ of Eq. 7 would have another factor of 2, and because $H_{r2}(r_2)$ of Eq. 2b must be zero, Eq. 5 would change to

$$H_{r2}(r,\phi) = I_V \frac{N}{r} \left[\left(\frac{r_1}{r} \right)^N - \left(\frac{r_1 r}{r_2^2} \right)^N \right] \cos N\phi \qquad (15a)$$

$$H_{\phi 2}(r,\phi) = I_V \frac{N}{r} \left[\left(\frac{r_1}{r} \right)^N + \left(\frac{r_1 r}{r_2^2} \right)^N \right] \sin N\phi \qquad (15b)$$

and W_1 would quadruple while W_2 would only double, giving a W_2/W_1 ratio only half that of Eq. 12a. The new L_1 of the inner gap region would be four times the value (Eq. 14a), which is about 3% lower than what we would expect as the number of vanes $2N \to \infty$.

Appendix B

Origin of Temperature-Rise Dependence

Assume a capacitor charges in T seconds and discharges in τ seconds, as shown in Fig. B-1. The heat dissipated in the capacitor is proportional to I^2. However, the temperature gradient depends upon the duty cycle, defined as $\frac{\tau}{T}$. Hence,

$$\Delta\text{Temp} \lesssim \left(\frac{I^2\tau}{T}\right).$$

Fig. B-1. Capacitor charge and discharge waveforms.

We define $P_{throughput} = \frac{1}{2} CV^2/T$ = average power handled by the capacitor.

We define $P_{discharge} = VI \approx \frac{1}{2} CV^2/\tau$.

$$\text{Then, } \Delta\text{Temp} \lesssim \left(\frac{I^2\tau P_{throughput}}{\frac{1}{2} CV^2}\right)$$

$$\lesssim \left(\frac{P_{throughput}\, I^2}{VI}\right).$$

Thus,

$$\Delta\text{Temp} \lesssim \left(\frac{P_{throughput}}{R_{discharge}}\right)$$

where $R_{discharge} = V/I$.

IMM/grw